

Politecnico di Torino



MASTER'S Degree in MECHANICAL ENGINEERING

MASTER'S Degree Thesis

STUDY OF THE TRANSMISSION IN HELICOPTERS FROM THE MAIN ROTOR TO THE TAIL

SUPERVISOR

Professor Teresa Maria Berruti

CANDIDATE

Giannis Hadjitheodoulou

JULY 2025

Abstract

This thesis aims to investigate the power transmission of helicopters from the engines to the tail rotor. The tail rotor is an essential component for the proper control of a helicopter. Even though different methods for the control of such vehicles have been developed, the tail rotor remains the principal solution for most modern helicopters.

In general, power transmission requires two gearboxes which allow translation in the direction of power coming from the main gearbox to the tail rotor, which is at a ninety-degree angle and possibly at a higher level with respect to driveshaft coming from the engines, as well as a speed reduction.

The main objective of this study is twofold; firstly, to study of the layout and assembly of the drivetrain and the gearboxes, and secondly, to design a tail rotor gearbox, based on an existing design, followed by a verification procedure, which involves the verification for static and dynamic loading on the components, the strength of the gear teeth, and the bearing life during operation. The verification is of high importance, to ensure the functionality and safety of the helicopter.

TABLE OF CONTENTS

Chapter 1	
Introduction to the Helicopter Transmission System	1
1.1 Purpose of the Helicopter Transmission System	2
1.2 Introduction to the Reference Helicopter	12
Chapter 2	
Component Analysis	15
2.1 Connection of the two Gearboxes	16
2.2 Intermediate Gearbox Assembly	17
2.3 Tail Rotor Gearbox Assembly	20
2.4 Pitch Angle Control Mechanism	22
Chapter 3	
Tail Rotor Gearbox Initial Design and Gear Verification	28
3.1 Initial Design of the Shafts	29
3.2 Input Shaft Gear Verification	36
3.3 Output Shaft Gear Verification	38
Chapter 4	
Bearing Selection and Verification	39
4.1 Bearing Selection	40
4.2 Rating Life Evaluation	45
4.3 Rating Life Considering Typical Missions	48
4.4 Completed Gearbox Design	50
Chapter 5	
Static and Fatigue Verification	53
5.1 Static Verification	54
5.2 Fatigue Verification	61
Closing Remarks	65
Annex 1	
Bearing Dynamic Life Evaluation Graphs and Tables	66
Annex 2	
Graphs for Fatigue Verification	74
Bibliography	82

Chapter 1

Introduction to the Helicopter Transmission System

1.1 Purpose of the Helicopter Transmission System

Helicopter transmission systems have the purpose of transferring power produced by reciprocating or, more typically, turboshaft engines, located above the fuselage, to one or more rotors to generate lift, control velocity, or produce an anti-torque effect.

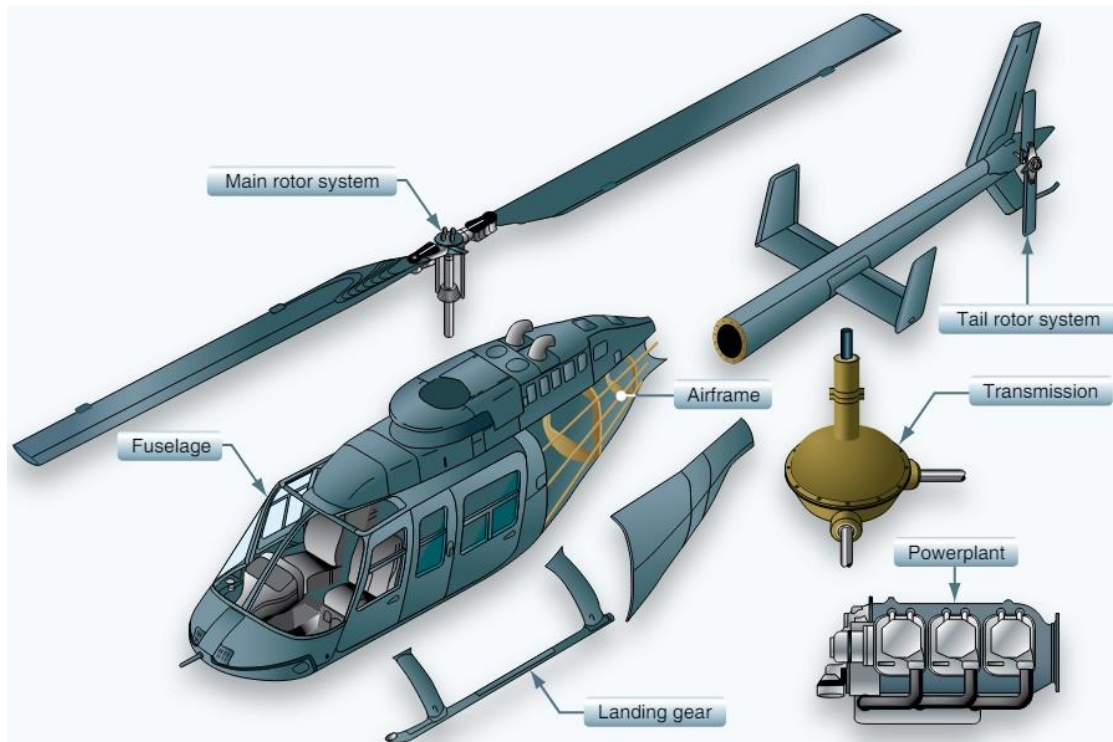


Figure 1.1 main components of a helicopter [2]

The main rotor system, located above the fuselage and near the engines, is used for the lift and for controlling the velocity and travel direction of the vehicle. It is connected to the engines through the main gearbox. The main gearbox transmits power from the engines, which are usually found in a horizontal position, through a first set of bevel gears at the first speed reduction stage, and then through a set of planetary gears, at the second stage, that finally lead to the mast, the shaft on which the blades of the main rotor are connected through a hub (**Fig.1.2**). The main gearbox also powers secondary gearboxes that may be required. In addition, the main gearbox assembly has a structural purpose, as its external case is directly connected to the fuselage. Therefore, aside from the loads coming from the bearings

supporting the shafts, the external case also supports the loads coming from the main rotor blades.

A centrifugal or a belt-drive clutch is located between the engine and the transmission, as the inertia of the transmission and the rotors is substantially high for the engine to start if they are connected during the starting transient [6].

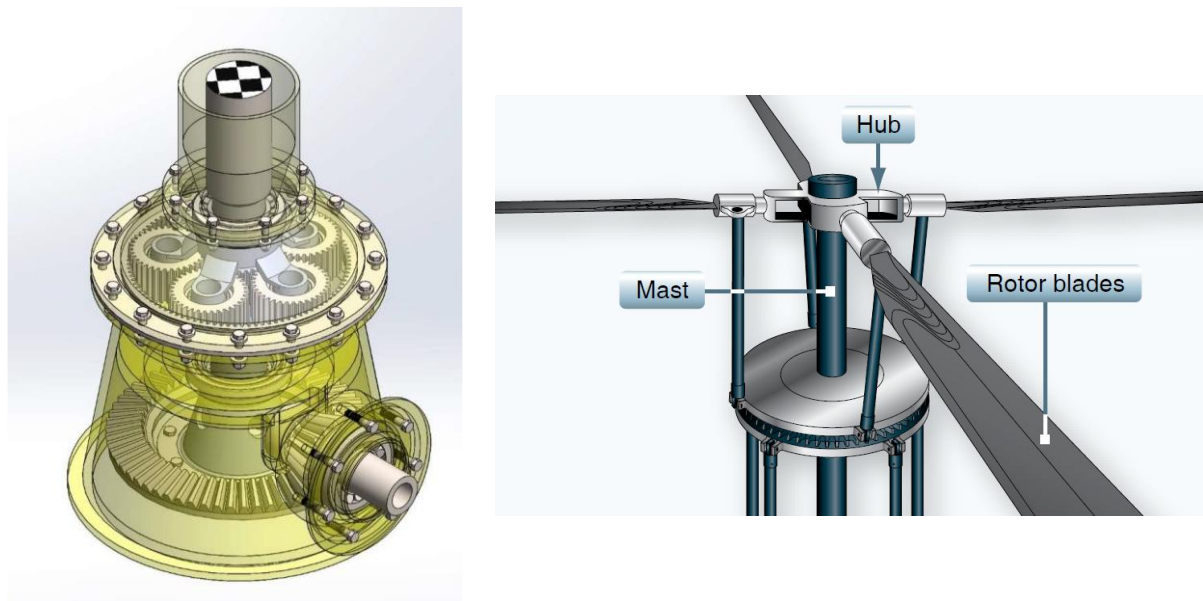


Figure 1.2 the main gearbox reduction stages and the connection to the main rotor [2]



Figure 1.3 the main gearbox of a Leonardo AW139

The main problem resulting from the rotation of the main rotor is that the torque applied on it produces equal and opposite torque on the fuselage of the helicopter itself, as expected by Newton's third law of equal and opposite forces. This would make the helicopter rotate in the opposite direction of the rotor. As a result, an antitorque solution should be applied when designing a rotorcraft.

One of the possible solutions is to have two main rotors, instead of just one, rotating in opposite directions to cancel out the torque that they generate on the airframe. The two rotors can be placed in tandem, coaxially, or in an intermeshing configuration. Using two main

rotors has the added advantage that more lift can be produced from shorter blades, allowing a higher payload capability.



Figure 1.4 a Kamov Ka-50 featuring a coaxial main rotor [26]

A more unusual solution, called NOTAR – short for no tail-rotor - was developed by McDonnell Douglas in the 1970s. It uses a variable pitch fan, connected to the engines, blowing air through two slots in the tail boom, to produce a lift force through the downwash of the main rotor going over the tail boom. This method exploits the Coanda effect. The counter-torque produced can be controlled though an additional jet-thrust at the end of the tail boom. This solution has the advantage of not requiring additional mechanical components such as long drive shafts and more gearboxes, which are typically needed by other antitorque methods.



Figure 1.5 an MD-600N helicopter using the NOTAR system [24]

However, the most used solution is to have a tail rotor producing thrust in the opposite direction to the torque produced by the main rotor. Regulation of the thrust can be achieved through the control of the pitch of the tail rotor blades and can be used for yaw control (rotation about the vertical axis). The fan can be either confined as in **Fig.1.7**, in what is called a “Fenestron”, or open as in **Fig.1.8**,

It is important to note that the power required for the tail rotor can range from 10% - during normal flight - to about 20% - at the extremes of the flight envelope- of the power required for the main rotor [32]. Thus, it can present a significant penalty on the power produced by the power units.

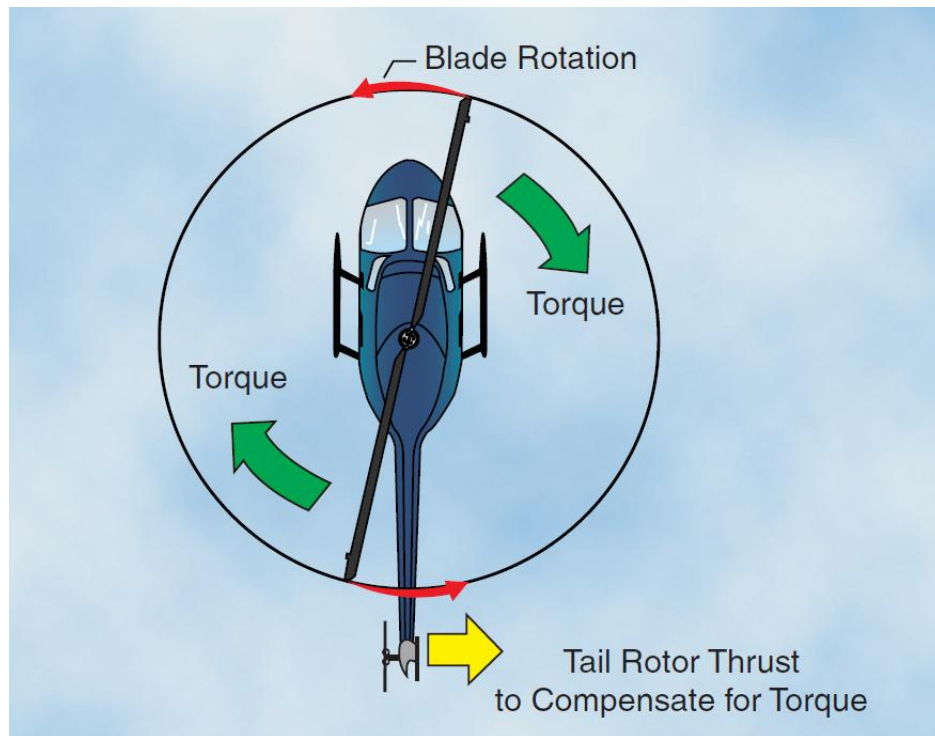


Figure 1.6 antitorque produced by the tail rotor [6]



Figure 1.7 a Cyprus Air Force Aerospatiale Gazelle featuring a Fenestron [4]



Figure 1.8 tail rotor from a Bell UH-1, with the linkages allowing the blade pitch control
[23]

The translation of power from the main gearbox to the tail rotor makes up the second part of the transmission system of a helicopter. This is achieved through the tail rotor driveshaft which is composed of segments connected by flexible plate couplings, such as the one shown by **Fig.1.10**, allowing a degree amount of axial misalignment between the shafts connecting to them.

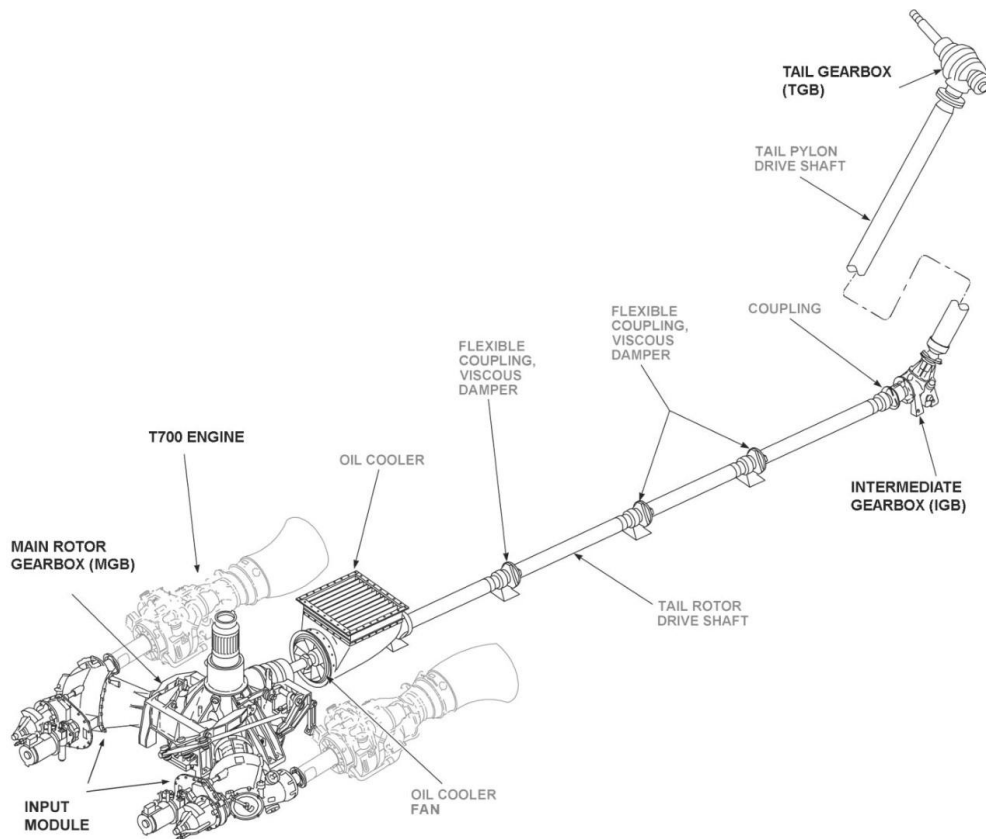


Figure 1.9 the complete transmission system of the Sikorsky H60 family of helicopters [22]



Figure 1.10 369D25501-9 Coupling used in the transmission of a MD 600 [8]

At the tail, a second gearbox is required to change the direction of rotation by 90 degrees. Thus, this gearbox is called a 90 degree or tail rotor gearbox. It also performs a speed reduction.

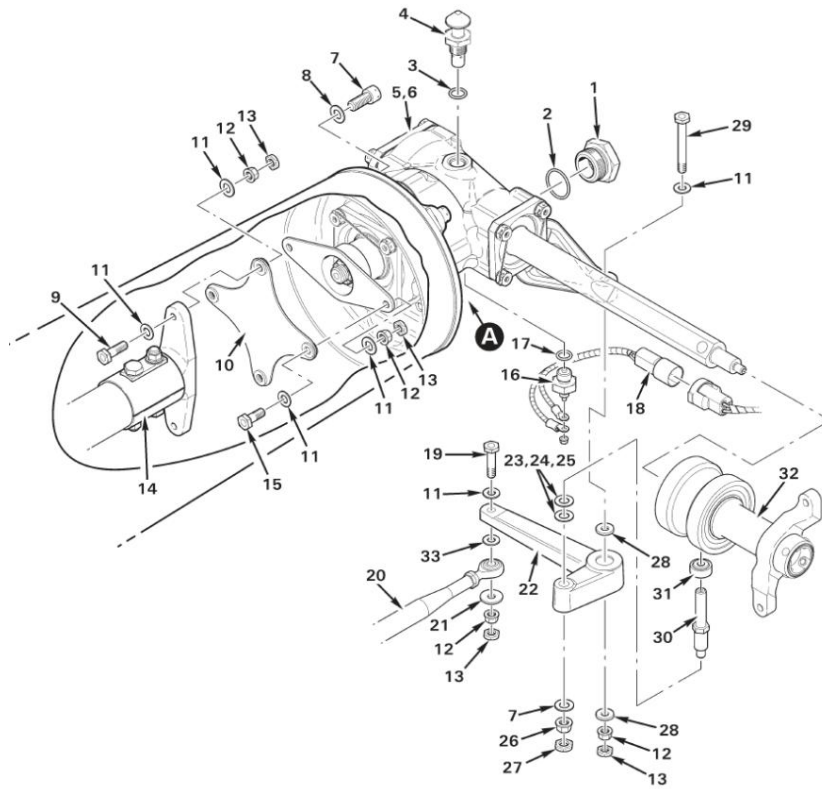


Figure 1.11 the tail rotor gearbox of a Robinson R44 [25]

If the tail rotor is exposed and not confined, to ensure that the rotor is protected from ground obstacles, and to reduce the risk to the ground crew, it can be placed higher on the tail. This requires an additional gearbox, known as an intermediate gearbox. As the name suggests, this gearbox is located between the main gearbox and the tail rotor gearbox.

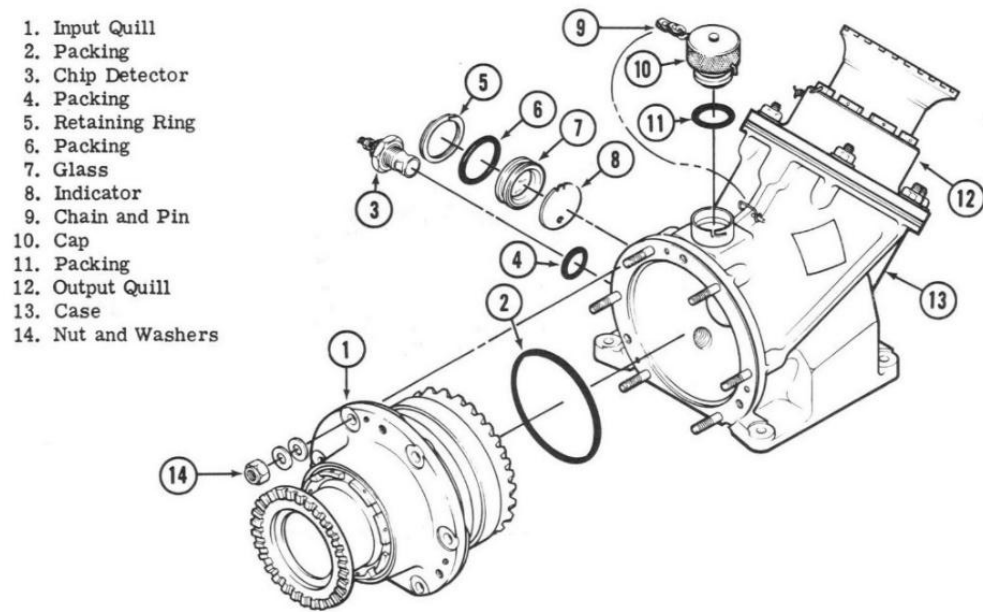


Figure 1.12 the intermediate gearbox of a Bell 205A-1 [7]

1.2 Introduction to the Reference Helicopter

Subsequent parts of this report deal with the design and the verification procedure on the input shaft of a tail rotor gearbox. The relevant dimensions and forces will be defined using the Bell UH-1H helicopter as reference.

The Bell UH-1 “Iroquois”, also called “Huey” due to its original designation being the HU-1, is a military utility helicopter produced by Bell Helicopter from the 1960s until the 1980s. It is mostly known for its use during the Vietnam war. It was the first design in the Huey range of helicopters that continue to be built to this day.



Figure 1.13 Vietnam war UH-1 helicopters [13]

The design of this helicopter is characterized by a two-blade main rotor and tail rotor. It uses a single turboshaft Lycoming T53 engine, that sits behind the main gearbox and above the tail rotor driveshaft, as shown by **Fig.1.13**. It employs an intermediate gearbox performing a 42-degree change in the direction of the driveshaft and a 90-degree tail rotor gearbox. Its main specifications are given by **Tab.1.1**.

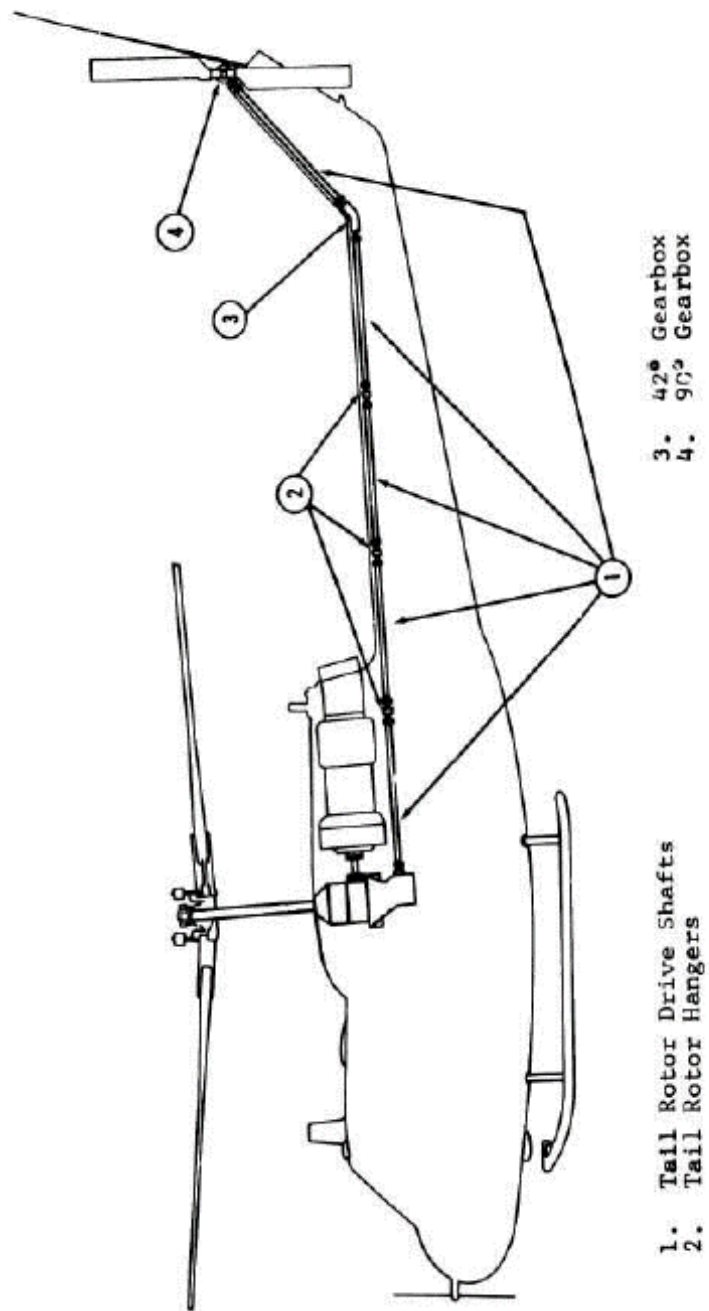


Figure 1.14 UH-1 powertrain layout [21]

Parameter	Symbol	Value
Max power	P_{\max}	1044 kW (single Lycoming T53 engine)
Maximum percentage of power in tail rotor	PP_{tail}	20%
Engine rotational speed	n_{eng}	6,600 RPM
Main rotor speed	n_{main}	324 RPM
Tail rotor speed	n_{tail}	1782 RPM
Max altitude	A_{\max}	12,000 feet \approx 3658 m
Max cruising speed	v_{\max}	117 knots \approx 217 km/h
Max mission duration	-	2 h
Max range	-	318 km
Max take-off mass	m_{\max}	9,500 lbs \approx 4300 kg
Max rate of climbing	ROC_{\max}	7.1 m/s
Gearbox material (assumed for study)	-	42CrMo4 steel
Tail rotor gearbox reduction ratio	t_1	2.14:1

Table 1.1 UH-1H main specifications [17]

Chapter 2

Component Analysis

2.1 Connection of the two Gearboxes

Fig.2.1 shows the connection between the gearboxes in the case of a helicopter with an elevated tail rotor. As stated in the first part of the report, power is transmitted from the main gearbox, through the tail rotor driveshaft, to the input shaft of the intermediate gearbox, which translates the power to the second part of the driveshaft, that is at an angle with respect to the first part. The second part of the driveshaft is connected to the input shaft of the tail rotor gearbox. Finally, the output shaft of the tail rotor gearbox powers the tail rotor, after the final translation of power by 90 degrees and a speed reduction.

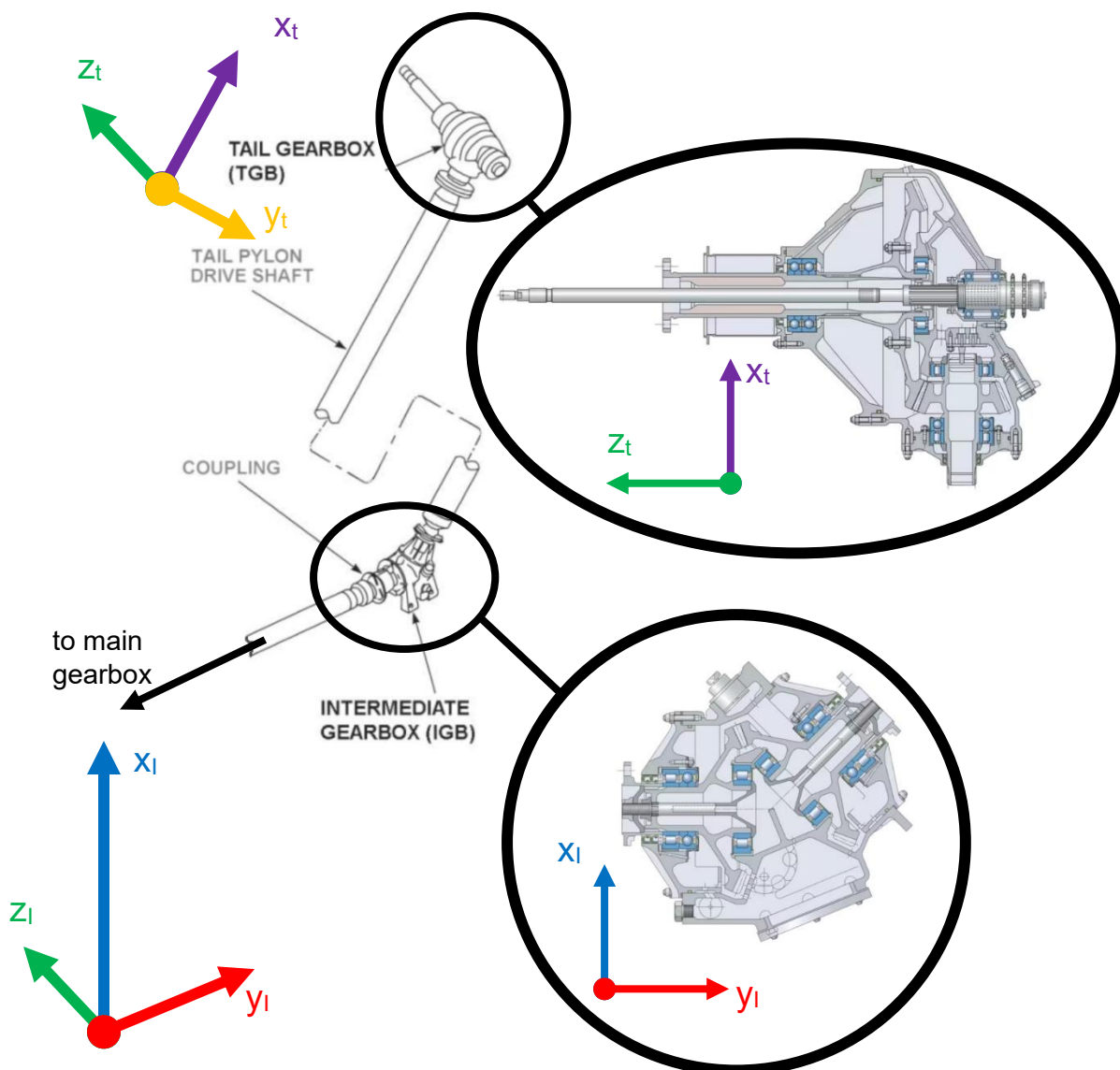


Figure 2.1 connection of intermediate gearbox and tail rotor gearbox [22][27][28]

2.2 Intermediate Gearbox Assembly

The intermediate gearbox employs two bevel gears with involute teeth profile to achieve a drive change of $40-45^\circ$, depending on the position of the tail rotor, with a gear ratio of 1:1, as its purpose is just a change in the direction of the driveshaft, and not a speed reduction.

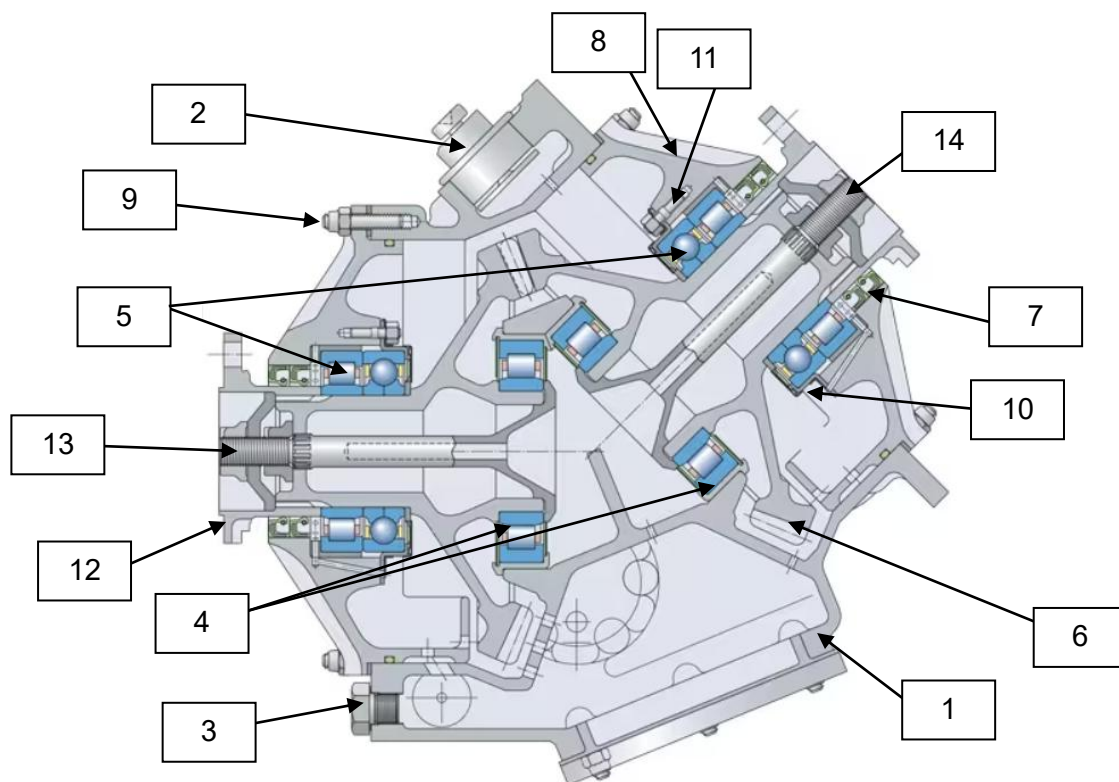


Figure 2.2 example of intermediate gearbox assembly [28]

#	Component Name	Quantity	Comment On Function
1	Casing	1	Holds bearings and shafts in place, contains lubricating oil
2	Vent cap	1	Releases internal pressure
3	Drain plug	1	Allows draining of oil
4	Non-locating bearings	2 (1 each shaft)	Provide radial reaction force, allow axial displacement
5	locating bearings	4 (2 each shaft)	Provide radial and axial reaction forces, fix the position of the shaft
6	Bevel gear	2	Transmit power with a drive change of around 45°
7	Rotary seals	4 (2 each shaft)	Prevent contaminants from entering inside
8	External cover	2 (1 each shaft)	Fix bearings and seals in place
9	External cover captive screws	12 (6 each shaft)	Hold external covers in place
10	Internal cover	2 (1 each shaft)	Fix bearings from the other side
11	Internal cover captive screws	12 (6 each shaft)	Hold internal covers in place
12	Coupling flanges	2 (1 each shaft)	Connect gearbox to the rest of the power transmission system
13	Input shaft	1	
14	Output shaft	1	

Table 2.1 Description of intermediate gearbox components (of **Fig.2.2**)

The two shafts are supported by cylindrical roller bearings at each end to counteract the radial loads, while another bearing is required to support the axial loads. In the figure seen above, that additional bearing is a four-point contact bearing. In this way, the side having the four-point contact bearing acts as the locating bearing, while the other side acts as the non-locating bearing. Instead of this setup, two tapered roller bearings, which have both axial and radial load carrying capabilities, could be used instead. In that case, preload would be required. The bearings are also protected from outside contaminants though seals. The outer raceway of the bearings is secured radially by the case, while their axial position is fixed by the flanges.

During operation, the gears can generate heat which will lead to an increase in the temperature of the oil and the air inside the case. This can lead to an increase in pressure in the case, which will in turn cause the oil to start leaking through the seals. Thus, a vent cap is required at the top of the gearbox, to counteract this effect.

The intermediate gearbox features a splash lubrication system [10]; the oil is transferred to the components through the rotation of the shafts. This means that no oil filters or pumps are used. The oil can move through the various parts of the gearbox through channels in the walls of the casing. Oil is generally inserted through a cap at the top of the gearbox near the pressure vent (not shown by **Fig.2.2** but shown by **Fig.1.12**) and is extracted from a drain plug at the bottom of the gearbox when an oil change is required.

To monitor the health of the system during operation, the gearbox has a magnetic chip detector (not shown by **Fig.2.2**) which attracts ferromagnetic chips produced through wear. The amount and type of chips collected by the detectors gives an indication of the wear inside the gearbox [20].

2.3 Tail Rotor Gearbox Assembly

As previously stated, the tail rotor or 90-degree gearbox aims to achieve a change in the direction of power by 90 degrees and a final speed reduction. In addition, the tail-rotor gearbox can be used to change the pitch of the tail-rotor blades. A possible layout for this gearbox can be seen in **Fig.2.3**.

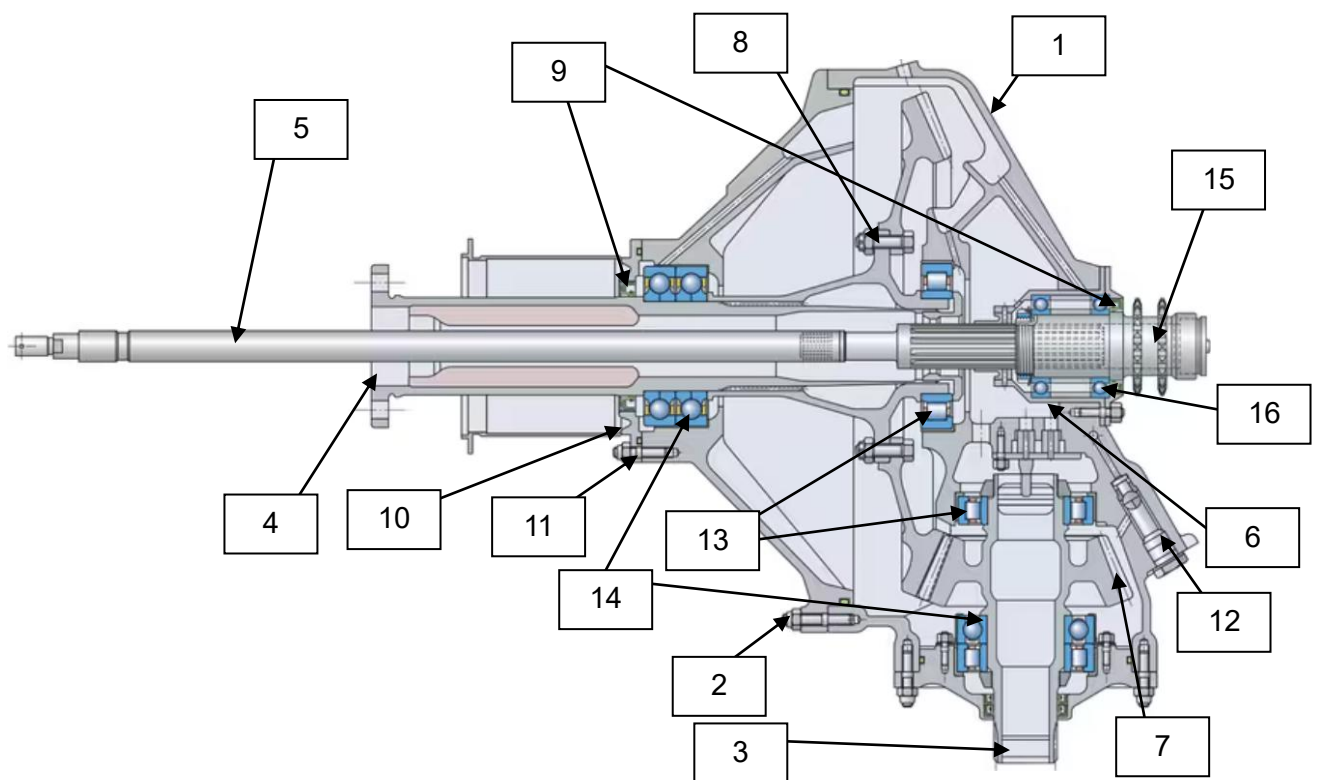


Figure 2.3 example of tail-rotor gearbox assembly [27]

#	COMPONENT NAME	QUANTITY	COMMENT ON FUNCTION
1	Casing	1	Holds bearings and shafts in place, contains lubricating oil
2	Casing captive screws	6	Hold together the two main parts of the casing
3	Input shaft	1	
4	Output shaft	1	
5	Control tube	1	Drives the crosshead connected to the pitch change links
6	Control quill	1	Supports control tube using a spline, allows relative rotation of the control nut
7	Bevel gear	2	Transmit power with a drive change of 90°
8	Bevel gear screws	6	Connect bevel gear of output shaft
9	Rotary seals	2 (1 each shaft)	Prevent contaminants from entering inside
10	External cover	2 (1 each shaft)	Fix bearings and seals in place
11	External cover captive screws	12 (6 each shaft)	Hold external covers in place
12	Chip detector	1	Detects wear level
13	Non-locating bearings	2 (1 each shaft)	Provide radial reaction force, allow axial displacement (simple supports)
14	locating bearings	4 (2 each shaft)	Provide radial axial reaction force, fix the position of the shaft (hinges)
15	Sprocket	1	Allows the rotation of the control nut using a chain
16	Control quill bearings	2	Allow relative rotation of the sprocket with respect to the control quill

Table 2.2 Description of tail rotor gearbox components (of Fig.2.3)

As in the intermediate gearbox and the main gearbox, a chip detector is included to give an indication of the amount and type of wear during operation.

Lubrication of the components is also achieved through an oil splash method, with channels inside the casing to allow lubricant to flow to more spatially restricted parts, such as the bearings supporting the output shaft.

2.4 Pitch Angle Control Mechanism

The angular speed of the rotors of a helicopter is constant throughout its operation. Thus, to increase or decrease the amount of lift produced by the main rotor, and the antitorque produced by the tail rotor, the angle of the rotor blades must be changed. Therefore, the tail rotor gearbox also includes a pitch change mechanism, that is actuated by the pilot through the operation of his antitorque pedals. In the case of the UH-1, the pedals are mechanically linked using a chain (which can be seen by **Fig.2.4**) as shown by **Fig.2.5**.



Figure 2.4 part of the pitch change mechanism control chain [29]

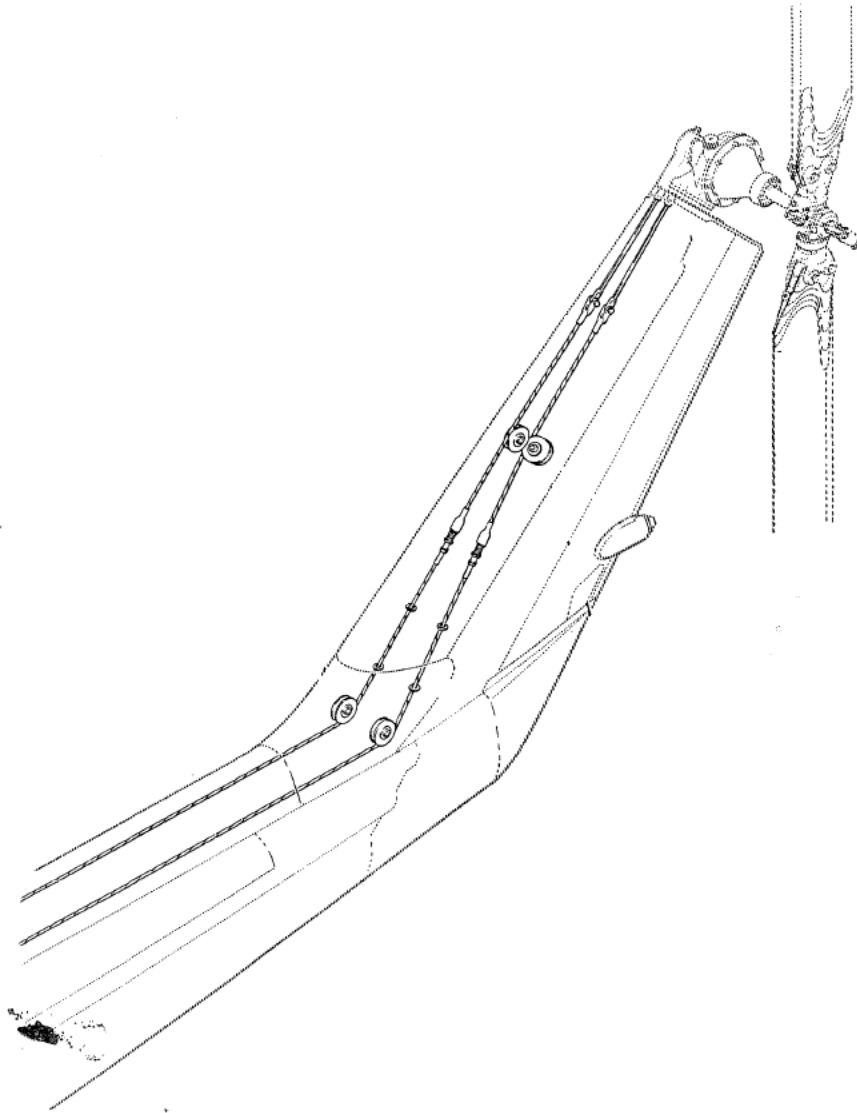


Figure 2.5 connection of the control chain through the tail to the tail rotor gearbox in the Bell UH-1 [7]

The main schematic of this mechanism in the UH-1 is shown by **Fig.2.6**. It is possible to see that the pitch change mechanism goes through the output shaft of the gearbox and changes the pitch angle of the blades using the pitch change links attached to them.

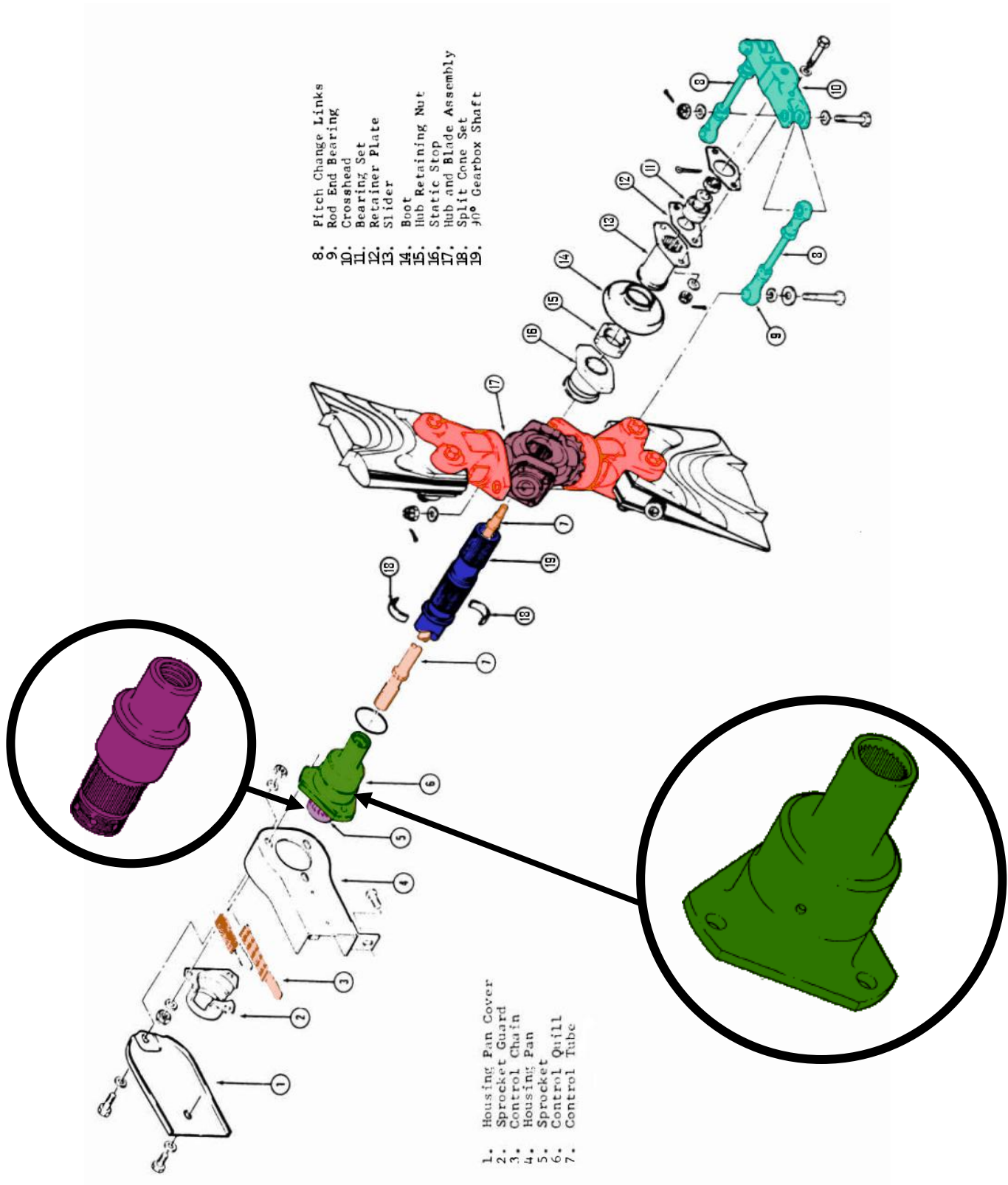


Figure 2.6 UH-1 tail rotor pitch change mechanism schematic [7][21]

The way this device works can be better understood through a 3D CAD reconstruction displayed by the following figures.

The blade angle is modified through the axial displacement of the control tube (colored yellow in the figures), which is connected to the blades through the crosshead and pitch change links (colored light blue). The control tube goes through the cavity of the output shaft of the helicopter (colored dark blue), that is partially represented by the 3D model. As can be seen, the output shaft supports the hub and blade assembly (red) using a spline.

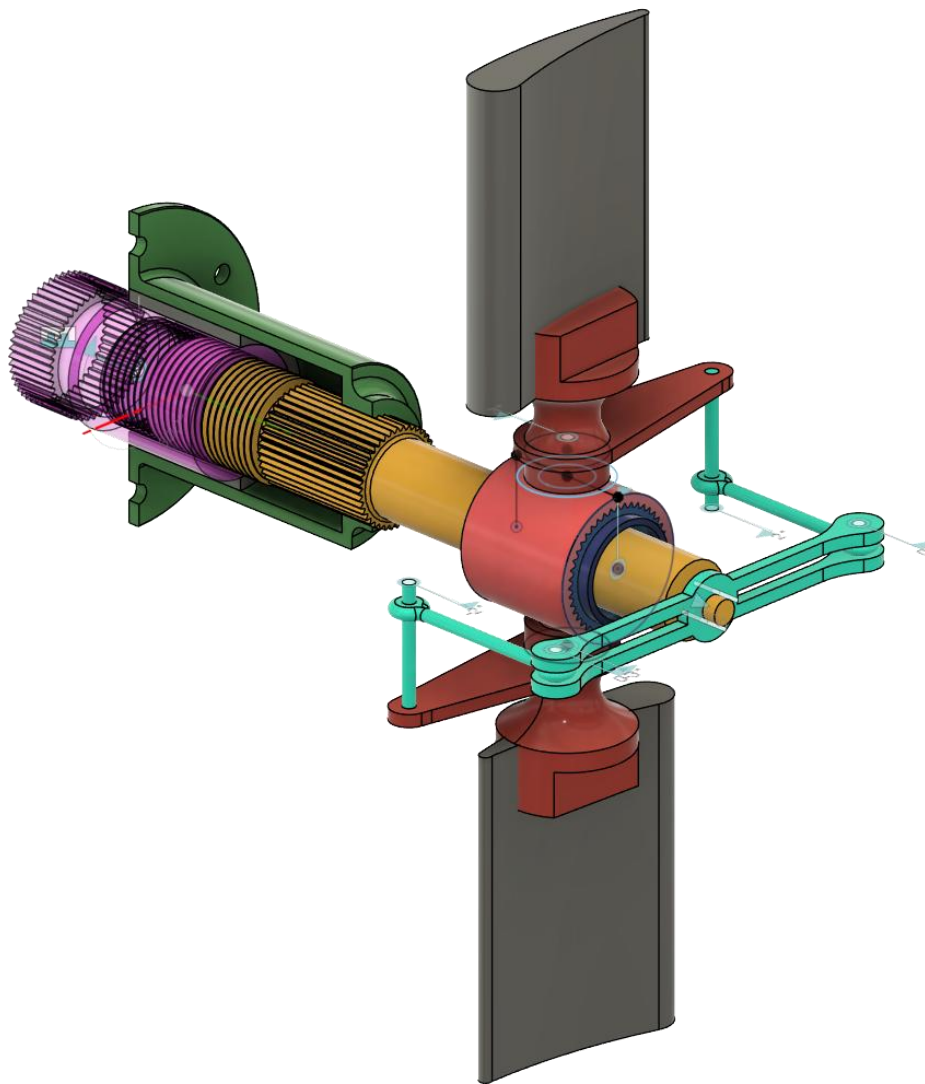


Figure 2.7 3D CAD reconstruction of the pitch change mechanism (not accurate dimensions)

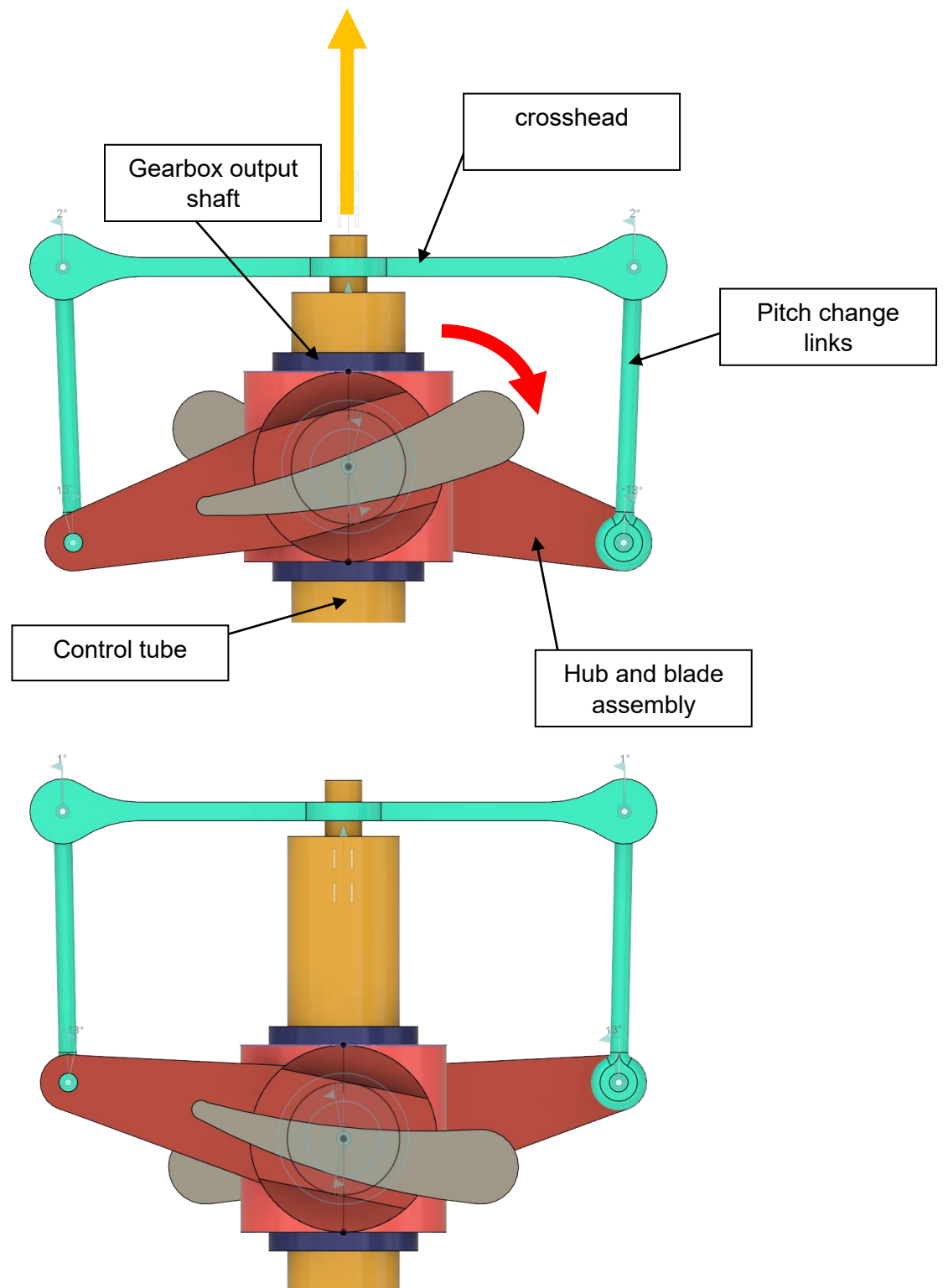


Figure 2.8 pitch angle change through the crosshead and pitch change links and control tube

The axial displacement of the control tube is achieved using a power screw mechanism; the control nut (purple) is rotated by the chain attached to it though a sprocket on the left end of the mechanism. The rotation of the nut is then translated into the axial displacement of the control tube. The control tube is radially constrained by the control quill (green) though a spline.

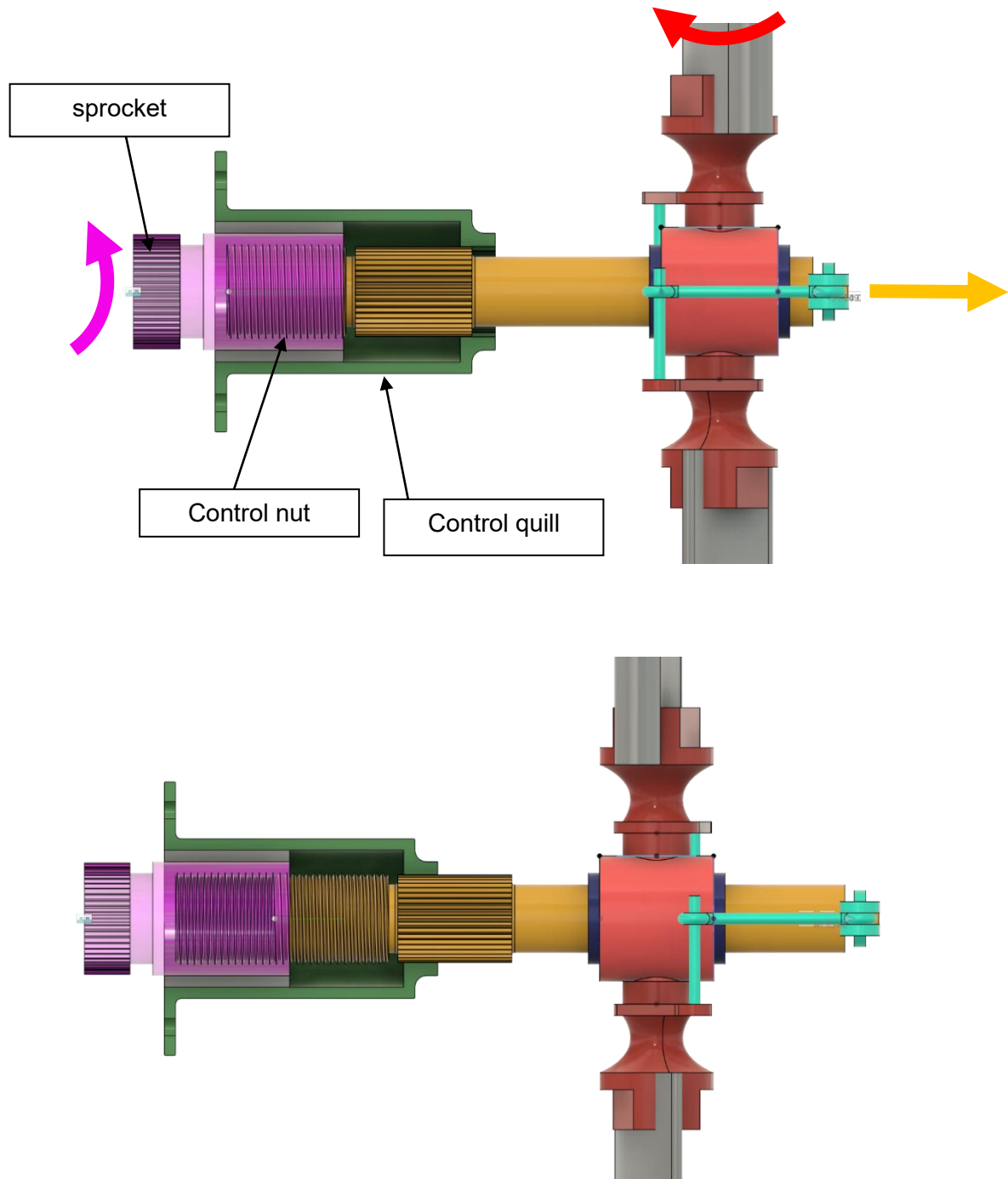


Figure 2.9 control tube axial displacement using a power screw mechanism

Chapter 3

Tail Rotor Gearbox Initial Design and Gear Verification

3.1 Initial Design of the Shafts

The design of the input shaft can be based on some of the engineering drawings provided by the original UH-1 maintenance manuals, internal part catalogues (IPCs), as well as available photographic material of the actual shafts. This will allow a preliminary design of the shafts and gears and their main characteristics.

The main design of the tail rotor gearbox is provided below.

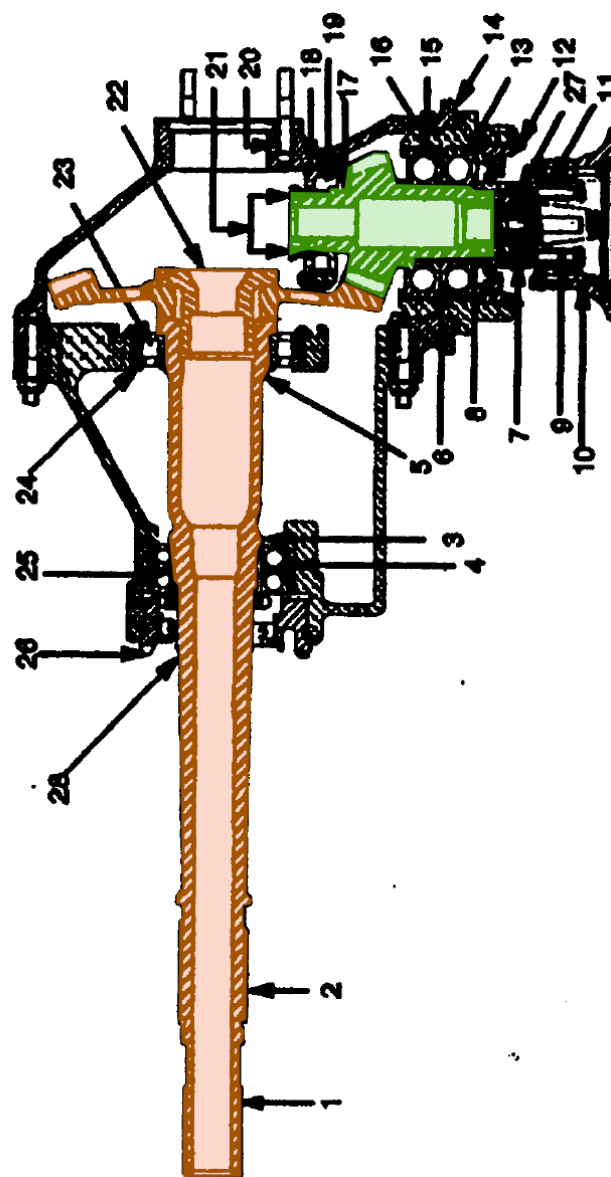


Figure 3.1 UH-1 tail-rotor gearbox drawing from original maintenance manuals showing input shaft (green) and output shaft (orange) [20]

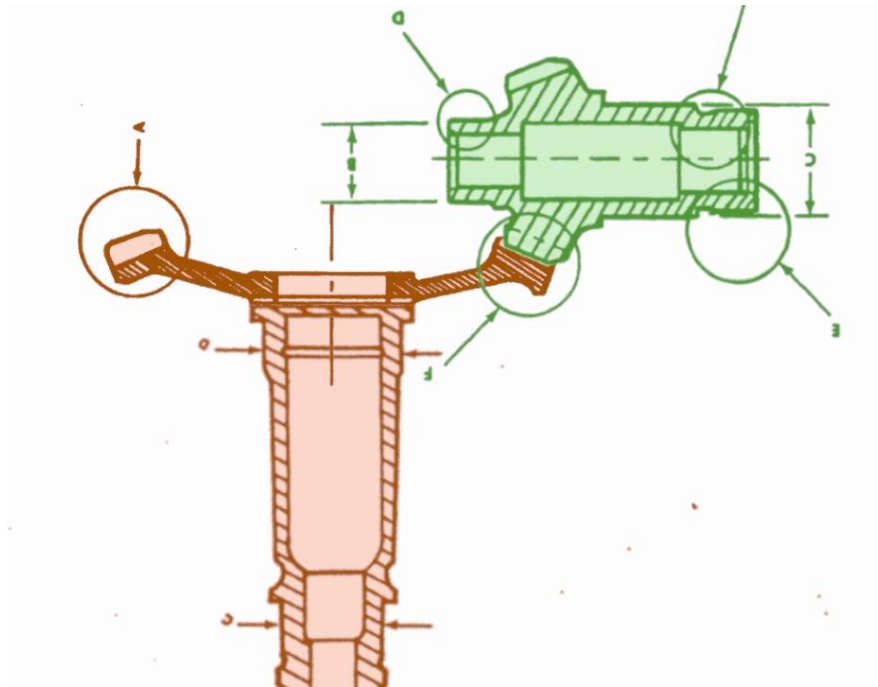


Figure 3.2 UH-1 tail-rotor gearbox input shaft (green) and output shaft (orange) detail from the original maintenance manuals [20]

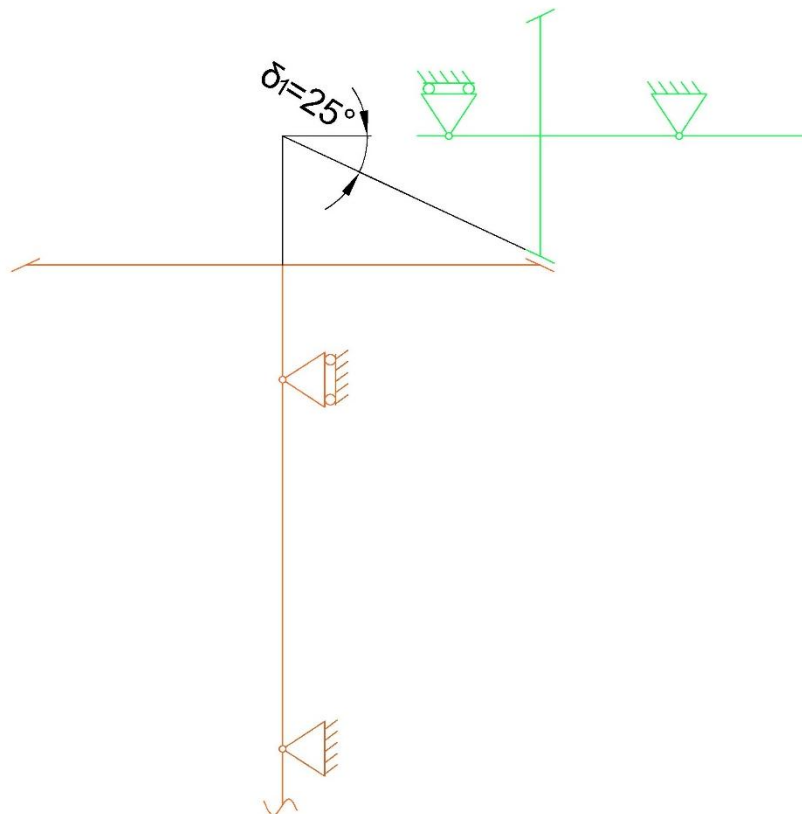


Figure 3.3 UH-1 tail-rotor gearbox simplified schematic

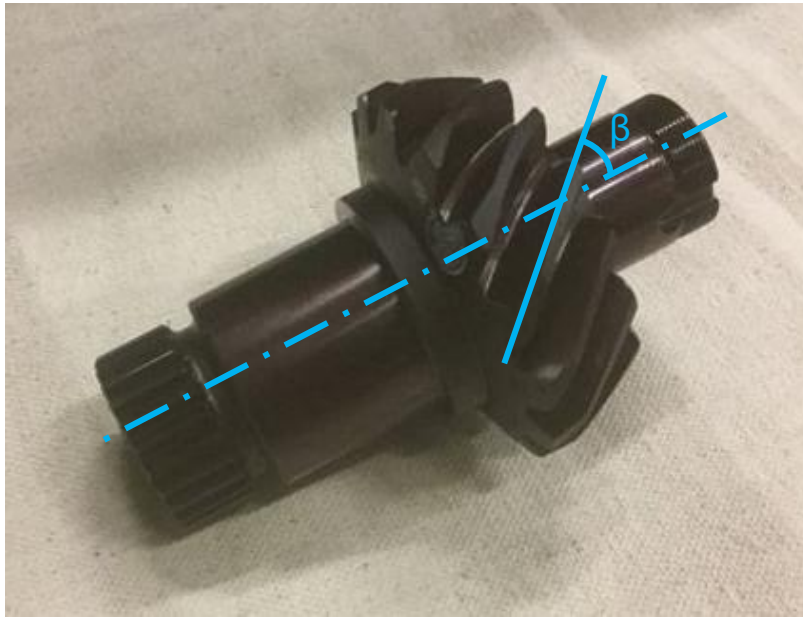


Figure 3.4 UH-1 tail-rotor gearbox input shaft [30]

Based on the drawings and the photographic material seen before, as well as some of the dimensions given by UH-1 technical manuals, the main gear characteristics, could be found and are given by the following tables.

Parameter	Symbol	value
Normal plane pressure angle	α_n	20°
Frontal plane pressure angle	α_t	24°
Helix angle	β	35°
Normal modulus	m_n	6 mm
Medium normal modulus	m_{nm}	5.0764 mm
Medium diameter tangential pitch	p_{tm}	19.47 mm
Tangential pitch	p_t	23.01 mm
Contact ratio	ε_a	1.87
Contact ratio	ε_b	1.13
Face width	b	37.35 mm
Pitch angle	δ_l	25°
Input shaft number of teeth	z_l	14
backbone diameter	d_l	102.54 mm
Pitch medium diameter	d_{lm}	86.7605
Input shaft gear generatrix	R	121.23 mm
Virtual number of teeth	z_{vl}	15.45
Normal plane virtual number of teeth	z_{vn1}	28.10
Profile shift	x_l	-
Addendum radius	r_{al}	52.94 mm
Base radius	r_{bl}	43.74 mm

Table 3.1 input shaft gear characteristics

Finally, preliminary drawings of the input and output shafts can be produced using AUTOCAD. The exact dimensions of the shaft as well as undercuts and other details will be determined after the selection of the rolling bearings, as they depend on the dimensions of the bearings themselves.

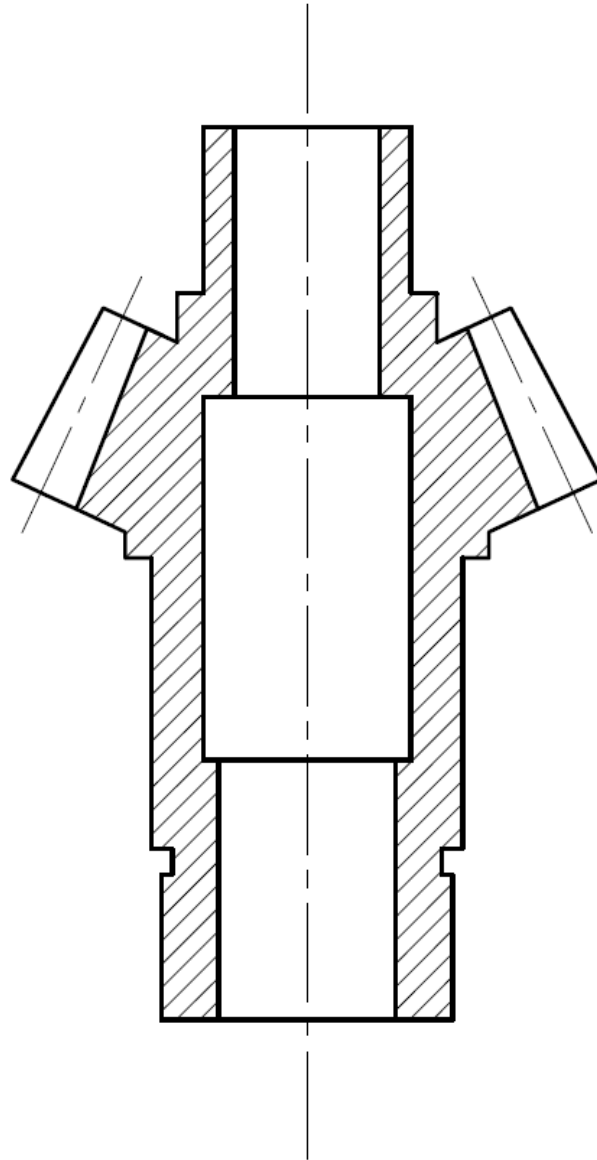


Figure 3.5 input shaft initial AUTOCAD drawing

Having found the pitch medium diameter and knowing the power and rotational speed of the tail rotor, the forces applied on the teeth can also be evaluated.

Parameter	Symbol	value
Input shaft torque	C_{input}	523 Nm
Tangential force	F_t	12053 N
Axial force	F_a	9912 N
Radial force	F_r	1287 N

Table 3.2 forces applied on the input shaft

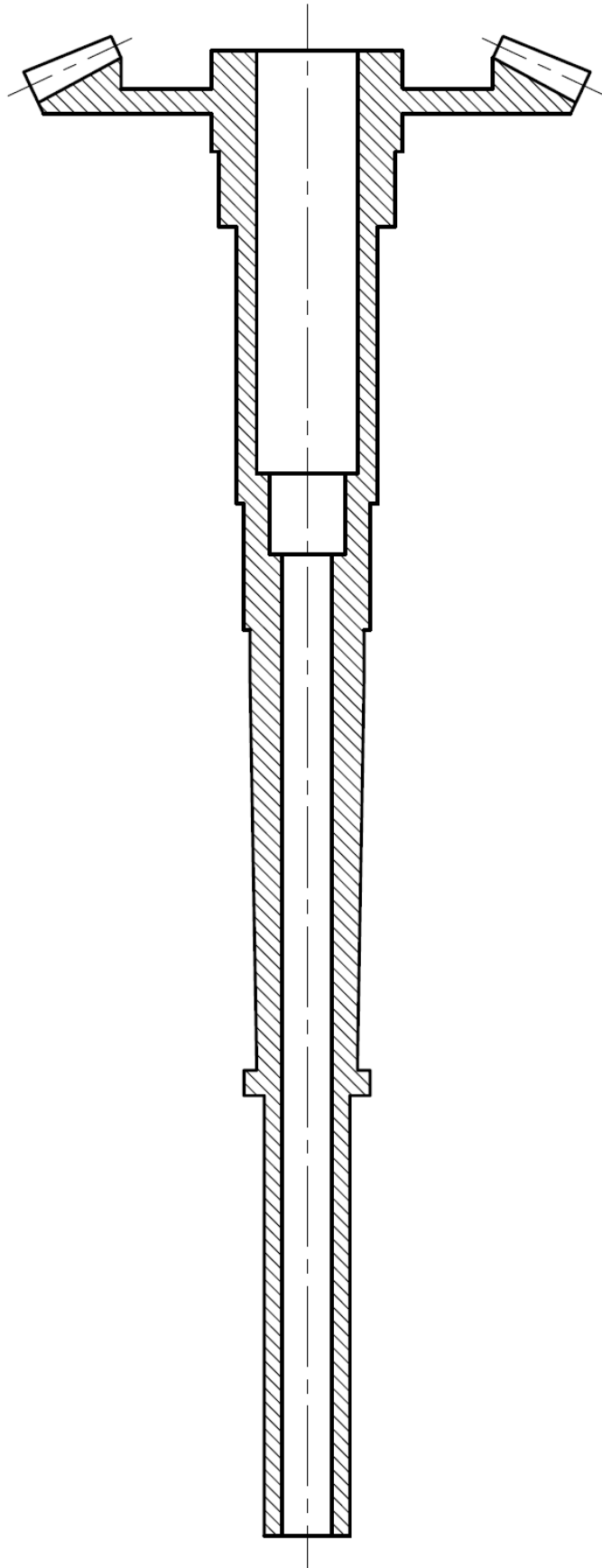


Figure 3.6 output shaft initial AUTOCAD drawing

Parameter	Symbol	value
Pitch angle	δ_2	65°
Input shaft number of teeth	z_2	30
backbone diameter	d_2	219.74 mm
Pitch medium diameter	d_{2m}	185.92 mm
Virtual number of teeth,	z_{v2}	70.99
Normal plane virtual number of teeth	z_{vn2}	129.15
Profile shift	x_2	-
Addendum radius	r_{a2}	225.03 mm
Base radius	r_{b2}	201.01 mm

Table 3.3 output shaft gear characteristics

3.2 Input Shaft Gear Verification

The verification of the gears was done according to the DIN Standards [33][34]. It involves the computation of two safety factors for each gear; the first one is the safety factor regarding the root of the teeth and the second one is about their flank surface.

Parameter	Symbol	value
Specific nominal pitch line force	w	322.70 N/mm
Dynamic factor	K_V	1.256
Overload factor	K_I	1.25 (assumed value)
Load distribution factor	$K_{F\alpha}$	1
Longitudinal load distribution factor	$K_{F\beta}$	1.2
Specific pitch line force	w_{Ft}	607.97 N/mm
Tooth form factor	Y_F	2.6455
Contact ratio coefficient	Y_ε	0.5338
Helical gear coefficient	Y_β	0.75
Tooth bending stress	σ_F	126.84 MPa
Allowable fatigue stress	σ_{FD}	420 MPa
Root safety factor	SF_{root}	3.31 > 1.8 (required value for infinite life)

Table 3.4 input shaft gear root safety factor parameters

Parameter	Symbol	value
Specific nominal pitch line force	w	As in Tab.3.4
Dynamic factor	K_V	As in Tab.3.4
Overload factor	K_I	As in Tab.3.4
Spur gear load distribution factor	$K_{H\alpha}$	1
Longitudinal load distribution factor	$K_{H\beta}$	1.2
Specific pitch line force	w_{Ft}	607.97 N/mm
Flank form factor	Z_H	1.5066
Material factor	Z_M	$272 \text{ (N/mm}^2\text{)}^{1/2}$
Contact ratio factor	Z_ϵ	0.6553
Tooth bending stress	σ_H	861 MPa
Allowable fatigue stress	σ_{HD}	1220 MPa
Surface safety factor	SF_{root}	1.42 > 1.4 (required value for infinite life for $z_1 \leq 20$)

Table 3.5 input shaft gear surface safety factor parameters

The gear is thus verified for both its root and surface strength.

3.3 Output Shaft Gear Verification

The verification process has been repeated for the output shaft of the gearbox. Once again, the gear is verified with both the root and the surface safety factors.

Parameter	Symbol	value
Specific nominal pitch line force	w	As in Tab.3.4
Dynamic factor	K_V	1.259
Overload factor	K_I	As in Tab.3.4
Load distribution factor	$K_{F\alpha}$	As in Tab.3.4
Longitudinal load distribution factor	$K_{F\beta}$	As in Tab.3.4
Specific pitch line force	w_{Ft}	608.74 N/mm
Tooth form factor	Y_F	2.1896
Contact ratio coefficient	Y_ϵ	As in Tab.3.4
Helical gear coefficient	Y_β	s in Tab.3.4
Tooth bending stress	σ_F	105.11 MPa
Allowable fatigue stress	σ_{FD}	420 MPa
Root safety factor	SF_{root}	4>1.8 (required value for infinite life)

Table 3.6 output shaft gear root safety factor parameters

Parameter	Symbol	value
Specific nominal pitch line force	w	As in Tab.3.4
Dynamic factor	K_V	As in Tab.3.6
Overload factor	K_I	As in Tab.3.4
Spur gear load distribution factor	$K_{H\alpha}$	1
Longitudinal load distribution factor	$K_{H\beta}$	1.2
Specific pitch line force	w_{Ft}	608.74 N/mm
Flank form factor	Z_H	As in Tab.3.5
Material factor	Z_M	As in Tab.3.5
Contact ratio factor	Z_ϵ	As in Tab.3.4
Tooth bending stress	σ_H	588.54 MPa
Allowable fatigue stress	σ_{HD}	1220 MPa
Surface safety factor	SF_{root}	2.07>1.25 (required value for infinite life for $z_2>20$)

Table 3.7 output shaft gear surface safety factor parameters

Chapter 4

Bearing Selection and Verification

4.1 Bearing Selection

The following part involves the selection of the bearings of the two shafts of the tail rotor gearbox and the life evaluation of the most loaded bearing of the input shaft. The selection of the bearings was done using the dimensions taken from the original drawings from the maintenance manuals of the UH-1. The type of bearings selected is not the same as in the original design.

The figure below shows the design of the two shafts, as seen in the previous part, including also the bearings. The bearing configuration chosen for the two shafts features a cylindrical roller bearing acting as the non-locating bearing on one side, and a combination of a cylindrical roller bearing and a four-point contact bearing acting as the locating support. In both bearing positions the cylindrical roller bearings are chosen without flanges on one of their rings, such that they allow axial displacement. In this way, the cylindrical roller bearings provide the radial reaction force while the four-point contact bearings provide the axial reaction force. To ensure that the four-point contact bearings are not under radial loads – which could cause separation of their inner ring – they must be mounted with a radial clearance between the outer ring and the casing bore. To prevent the outer ring of the four-point contact bearings from turning, it is fixed in place by locating pins inserted in the locating slots of the ring.

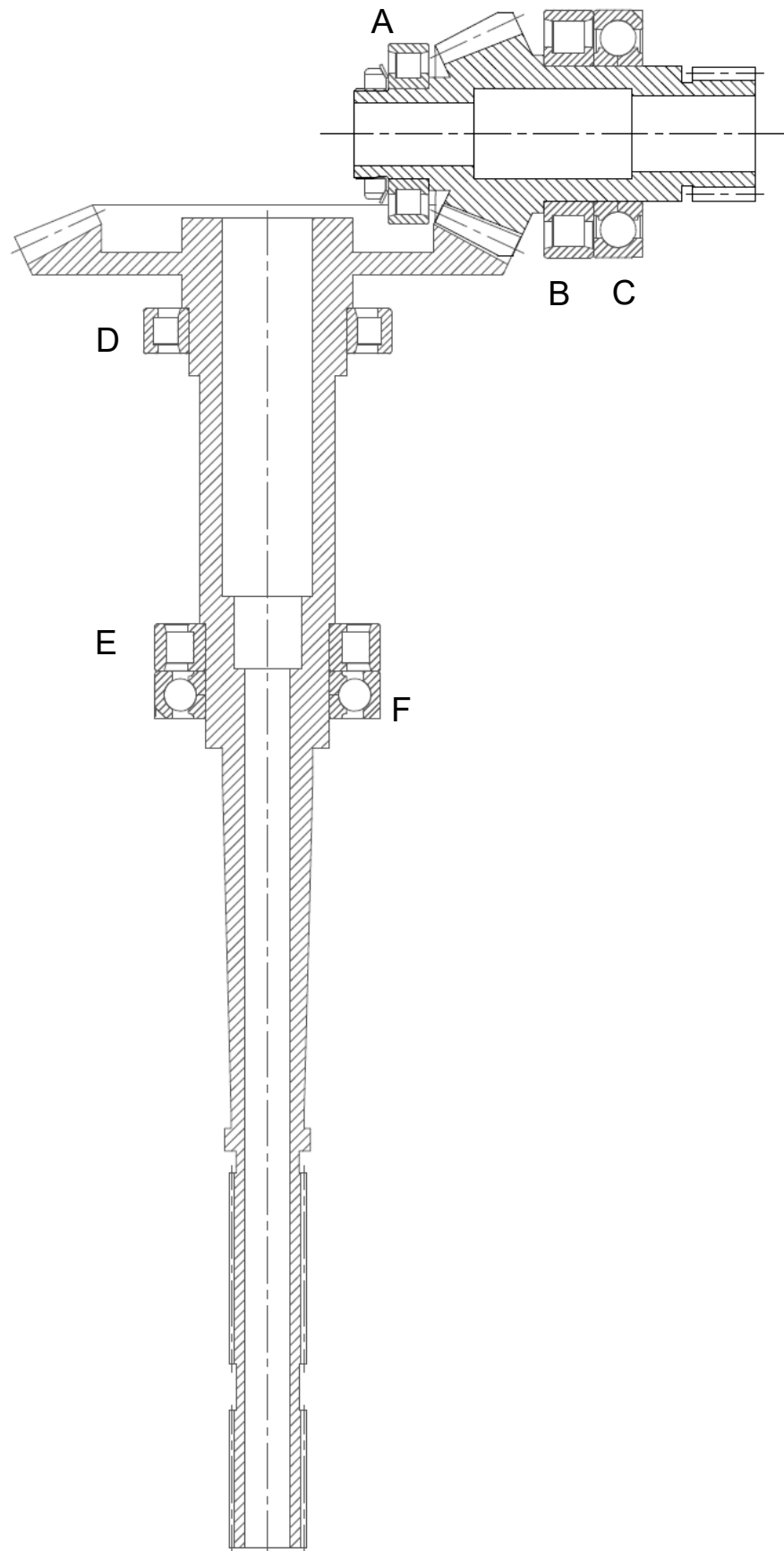



Figure 4.1 shafts design including the bearings

The tables below show the specifications of the bearings chosen for the input and output shafts.



SKF performance class		SKF Explorer
Basic dynamic load rating	C	62 kN
Basic static load rating	C ₀	53 kN
Fatigue load limit	P _u	6.7 kN
Reference speed		9 500 r/min
Limiting speed		11 000 r/min
Minimum load factor	k _r	0.12
Limiting value	e	0.2
Calculation factor	Y	0.6

Table 4.1 Bearing A (SKF N 208 ECP) calculation data [31]



SKF performance class		SKF Explorer
Basic dynamic load rating	C	108 kN
Basic static load rating	C ₀	102 kN
Fatigue load limit	P _u	13.4 kN
Reference speed		6 700 r/min
Limiting speed		7 500 r/min
Minimum load factor	k _r	0.12
Limiting value	e	0.2
Calculation factor	Y	0.6

Table 4.2 Bearing B (SKF N 212 ECM) calculation data [31]




SKF performance class		SKF Explorer
Basic dynamic load rating	C	96.5 kN
Basic static load rating	C ₀	93 kN
Fatigue load limit	P _u	4 kN
Limiting speed		10 000 r/min
Calculation factor	A	0.0242
Limiting value	e	0.95
Calculation factor	X	0.6
Calculation factor	Y ₀	0.58
Calculation factor	Y ₁	0.66
Calculation factor	Y ₂	1.07

Table 4.3 Bearing C (SKF QJ 212 N2MA) data [31]



SKF performance class		SKF Explorer
Basic dynamic load rating	C	86.5 kN
Basic static load rating	C ₀	93 kN
Fatigue load limit	P _u	12 kN
Reference speed		7 000 r/min
Limiting speed		7 000 r/min
Minimum load factor	k _r	0.1
Limiting value	e	0.2
Calculation factor	Y	0.6

Table 4.4 Bearing D (SKF NU 1014 ECP) data [31]



SKF performance class		SKF Explorer
Basic dynamic load rating	C	96.5 kN
Basic static load rating	C ₀	95 kN
Fatigue load limit	P _u	12.2 kN
Reference speed		7 500 r/min
Limiting speed		8 000 r/min
Minimum load factor	k _r	0.12
Limiting value	e	0.2
Calculation factor	Y	0.6

Table 4.5 Bearing E (SKF 211 ECP) data [31]



Calculation data

Basic dynamic load rating	C	159 kN
Basic static load rating	C ₀	196 kN
Fatigue load limit	P _u	22.8 kN
Reference speed		4 800 r/min
Limiting speed		5 600 r/min
Limiting value	e	0.28
Calculation factor	Y	2.1
Calculation factor	Y ₀	1.1

Table 4.6 Bearing F (SKF QJ 211 N2MA) data [31]

4.2 Rating Life Evaluation

Considering **Fig.4.1**, the distances between the gears and the bearings could be obtained, thus, allowing the computation of the force that each bearing must exert. The forces on each bearing are shown by the table below. It is evident that bearing C is the most loaded bearing, which could be expected considering that it supports all the axial force from the pinion gear, while the radial force is supported by the other two bearings.

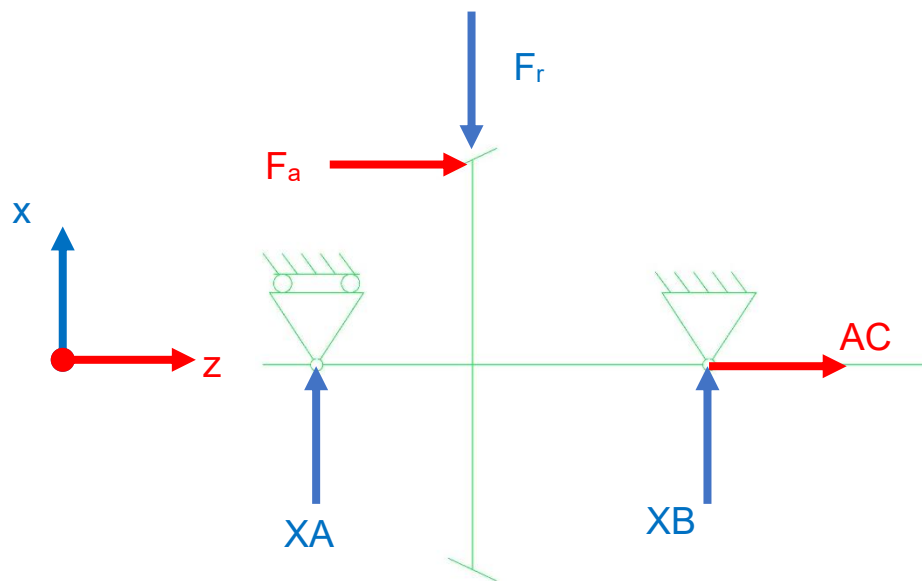


Figure 4.2 representation of the forces applied on the input shaft

Bearing	Force Direction	Symbol	Magnitude [N]
A	radial	RA	8774
B	radial	RB	7269
C	axial	AC	9912

Table 4.7 input shaft bearing reaction forces

The evaluation of the bearing life is done considering constant maximum power and using ISO 281:1 2000, whose expressions are given in Annex 1. The life of the bearing according to this technical standard, depends on several coefficients and parameters. When choosing these parameters, several considerations were made:

1. the gearbox does not feature oil filtering, and it is exposed to the environment, while the helicopter itself is used for military applications. This led to considering typical contamination when selecting the contamination factor.
2. Considering the severity of a potential failure (loss of vehicle control) the life adjustment factor was chosen to have a reliability level of 99%. This has led to a very conservative life estimation.
3. The oil temperature which is necessary for evaluating its viscosity and thus effecting the life estimation could not be known for this helicopter type. However, using data from a NASA report on the oil temperature of the UH-60A helicopter [18], it was assumed to be at 60°C.

The choice of coefficients is then reported below.

Coefficient	Symbol	Chosen Value
Contamination factor	η_c	0.3
Life adjustment factor	a_1	0.25
Oil temperature	T_{oil}	60 °C

Table 4.8 bearing life evaluation coefficients

Finally, the values of the dynamic bearing life could be evaluated, and they are reported by the next table in number of cycles and hours.

Bearing	Life [million cycles]	Life [hours]
A	5099	22256
B	21,479	93750
C	868	3789

Table 4.9 dynamic bearing life evaluation for input shaft bearings

According to the maintenance manuals of the UH-1, the frequency between scheduled maintenance for the tail rotor gearbox is 100 hours. It is then obvious that all three bearings cover this requirement when constant power is considered. It can also be observed that bearing C has the shortest life out of the three bearings.

4.3 Rating Life Considering Typical Missions

The previous evaluation was done considering constant power input. However, the provided power is not always constant. To perform the computation of the bearing life under variable power conditions it is possible to consider a typical mission of this helicopter type, shown by the figures below, showing the outbound leg and inbound leg of its mission. The figures include the distances and height that the UH-1 is expected to cover, as well as its cruising speed (CS), rate of climb (RoC) and rate of descent (RoD). The missions considered take into account the data provided by **Tab.3.1.** and the altitudes of Vietnam, where the UH-1 was used. The following life evaluation was only performed on bearing C, since it is the bearing with the shortest life.

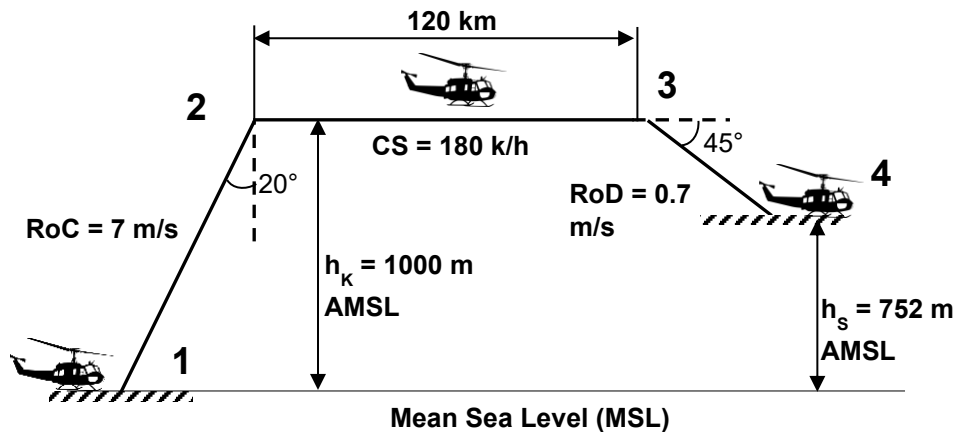


Figure 4.3 examined mission outbound leg

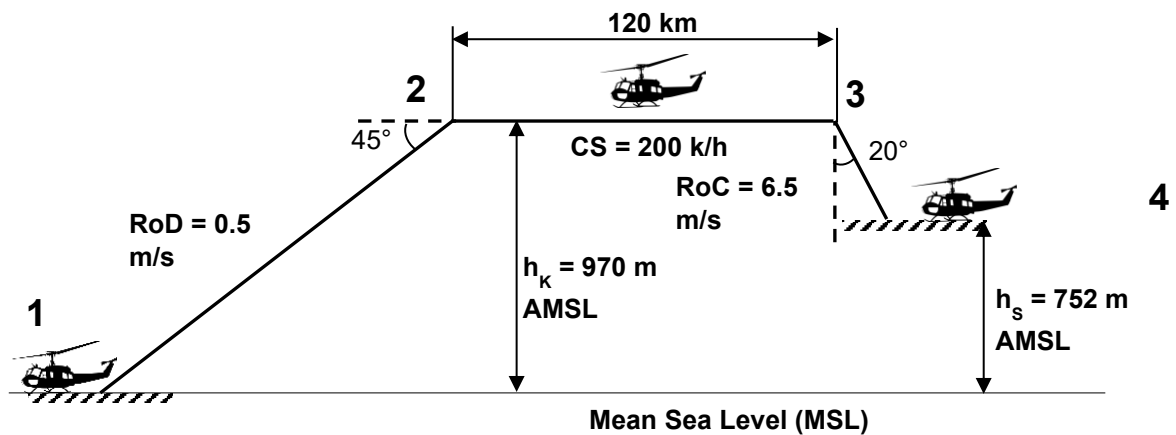


Figure 4.4 examined mission inbound leg

The percentage of maximum power and the resulting axial force produced by bearing C is presented in the table below. During take-off maximum power is used, and it is reduced for subsequent stages. The angular speed on the other hand is kept constant in all stages, with only the pitch angle of the blades determining the amount of lift produced by the main rotor and the anti-torque produced by the tail rotor. The travel time of each stage of the mission is also given by the table. The life rating for each individual mission stage was found in the same manner as in the condition examined in the previous part of the report, assuming that the power of each stage is constant. Having computed each life rating, the final life rating, considering the power changes could be computed. The life rating during maximum power stages in the take-off is the same as before. The other mission stages were re-examined separately.

Mission stage	path	% max power	Axial force of bearing C [N]	Life [million cycles]
1	1→2	100%	9912	868
2	2→3	85%	8425	1518
3	3→4	75%	7434	2330
4	4→3	100%	9912	868
5	3→2	90%	8921	1250
6	2→1	75%	7434	2330

Table 4.10 bearing life individual evaluation for each mission stage

Therefore, bearing C can last for around 3900 hours, which is the equivalent of around 4776 missions like the one shown above, before needing to be replaced. It is important to note that since 99% reliability is considered and that the power going to the tail rotor is at 20% which is higher than the power used most of the time, this estimation is conservative.

4.4 Completed Gearbox Design

Having selected the bearings, the design of the casing of the gearbox as the rest of the components holding the shafts and the bearings together can be completed

Looking at the drawing below, several observations can be made.

1. the teeth of the pinion gear feature a slight cut at the backbone diameter. This is done to ensure that the gear is smaller than the outer diameter of the bearings such that it can be fitted inside the casing from the outside. This can be also seen in **Fig.3.4**.
2. the four point contact bearings are fixed in place using spacers, which are also used to prevent their outer ring from turning using the locating pins, as they are assembled with radial clearance to ensure that no radial load is applied to them. The spacers are secured using nuts.
3. The main casing is composed of two parts, to allow the output shaft to be mounted from the inside.
4. The casing uses captive screws and self-locking nuts [7][20]. This allows disassembly by removing the nuts located on the outside of the casing, without having to remove the studs from the casing itself. Thus, the thread of the casing is more difficult to damage. The self-locking nuts are also harder to loosen under the vibrations produced by the helicopter during operation, compared to using normal screws instead.
5. The shafts feature splines at their ends. The spline on the input shaft is used to connect it to the coupling which transfers power from the rest of the system. The spline on the output shaft is instead used to support the hub and blade assembly as seen in Chapter 2.
6. The captive screws at the top end of the drawing of **Fig.4.5** are used to connect the pitch change mechanism seen in Chapter 2.

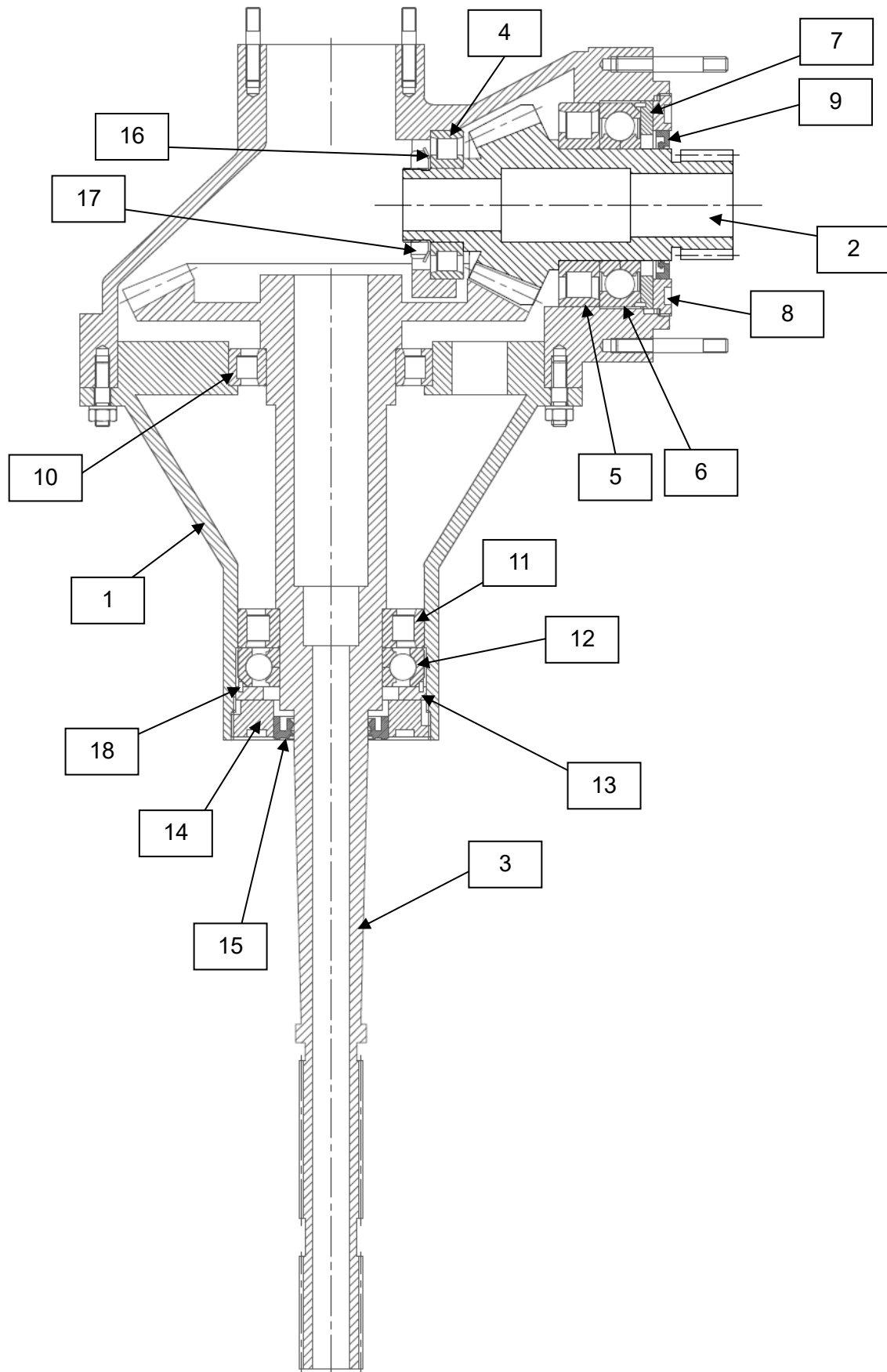


Figure 4.5 complete gearbox design after bearing life rating evaluation

#	Component Name	Code	Quantity
1	Casing	-	1
2	Input shaft	-	1
3	Output shaft	-	1
4	Input shaft non-locating cylindrical roller bearing	SKF N 208 ECP	1
5	Input shaft locating cylindrical roller bearing	SKF N 212 ECM	1
6	Input shaft four-point contact bearing	SKF QJ 212 N2MA	1
7	Input shaft spacer	-	1
8	Input shaft nut	-	1
9	Input shaft seal	SKF HMS5 60x80x7	1
10	output shaft non-locating cylindrical roller bearing	SKF NU 1014 ECP	1
11	output shaft locating cylindrical roller bearing	SKF 211 ECP	1
12	output shaft four-point contact bearing	SKF QJ 211 N2MA	1
13	Output shaft spacer	-	1
14	Output shaft nut	-	1
15	Output shaft seal	SKF HMS5 40x62x10	1
16	Lock washer	SKF MB 8	1
17	Lock nut	SKF KM 8	1
18	Locating pin		4

Table 4.11 tail rotor gearbox components (referring to **Fig.4.5**)

Chapter 5

Static and Fatigue Verification

5.1 Static Verification

Having verified the gear design and the bearings of the 90-degree gearbox input shaft, it is also important to verify that it is able to support the loads applied to it. The three loading modes applied to the shaft will be:

1. Compression: between the gear force application point and bearing C, due to the axial force produced by the gear and the corresponding bearing reaction force
2. Bending: between the bearings A and B as the gear is subjected to the radial and tangential loads
3. Torsion: between the gear and the spline at the end of the shaft through which the power is transmitted

The first step is to compute the internal actions acting in the shaft.

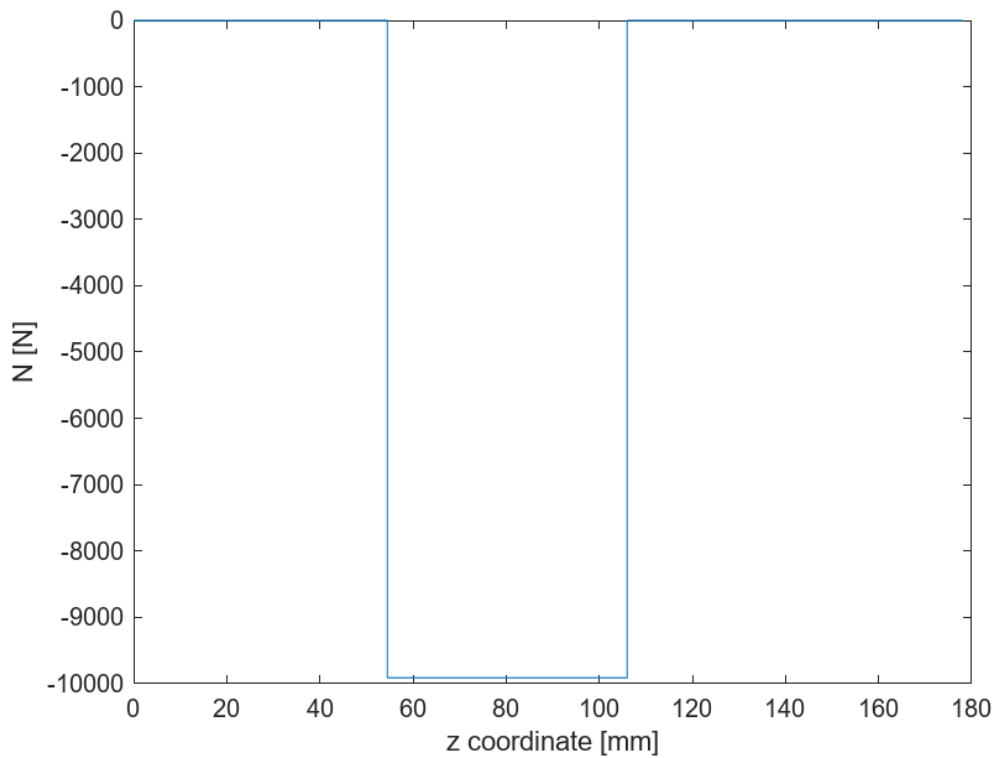


Figure 5.1 axial loads acting on the shaft

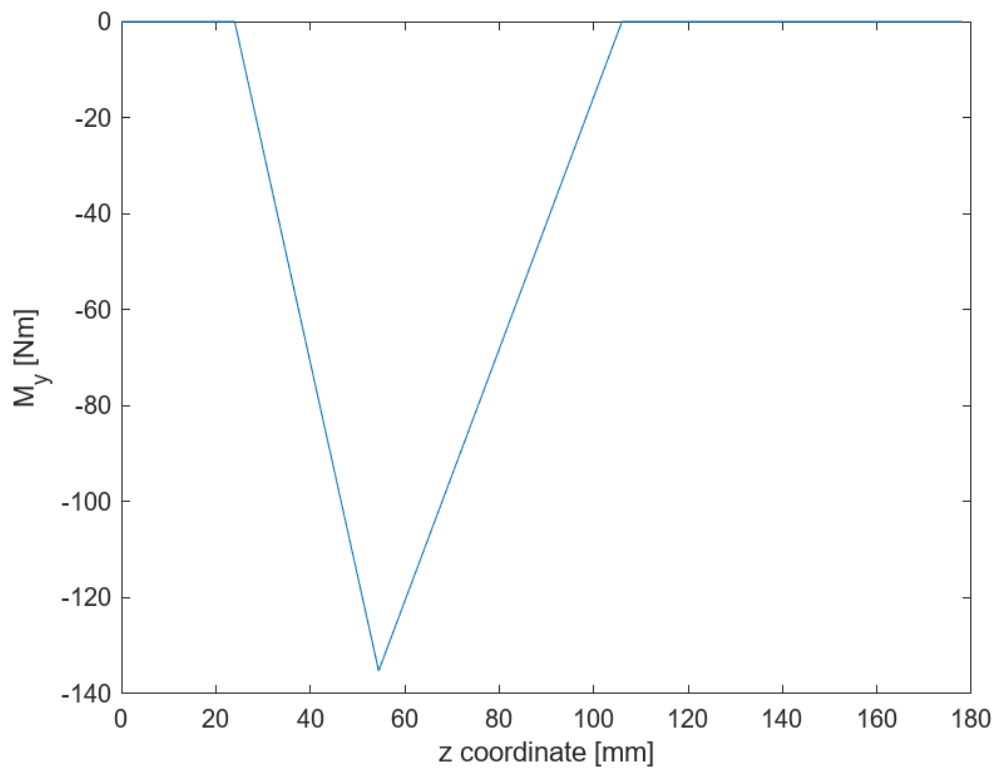


Figure 5.2 bending loads acting on the shaft

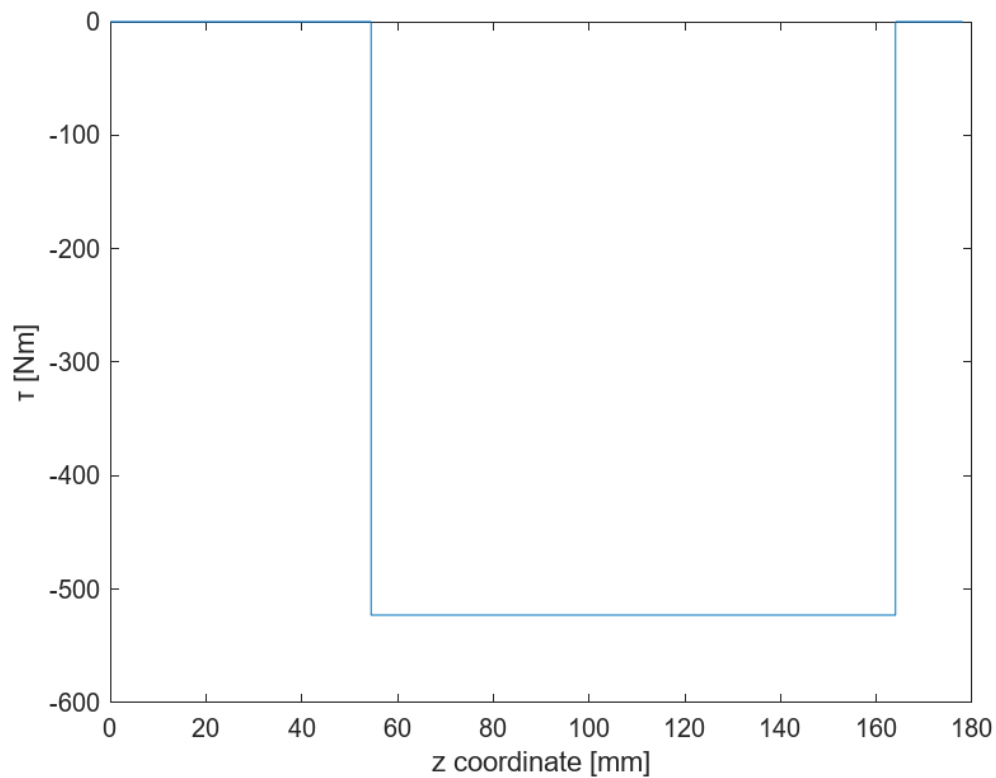


Figure 5.3 torsional loads acting on the shaft

The stresses produced because of these loads depend on the geometry of the shaft; its cross-sectional area and the bending and torsion section moduli.

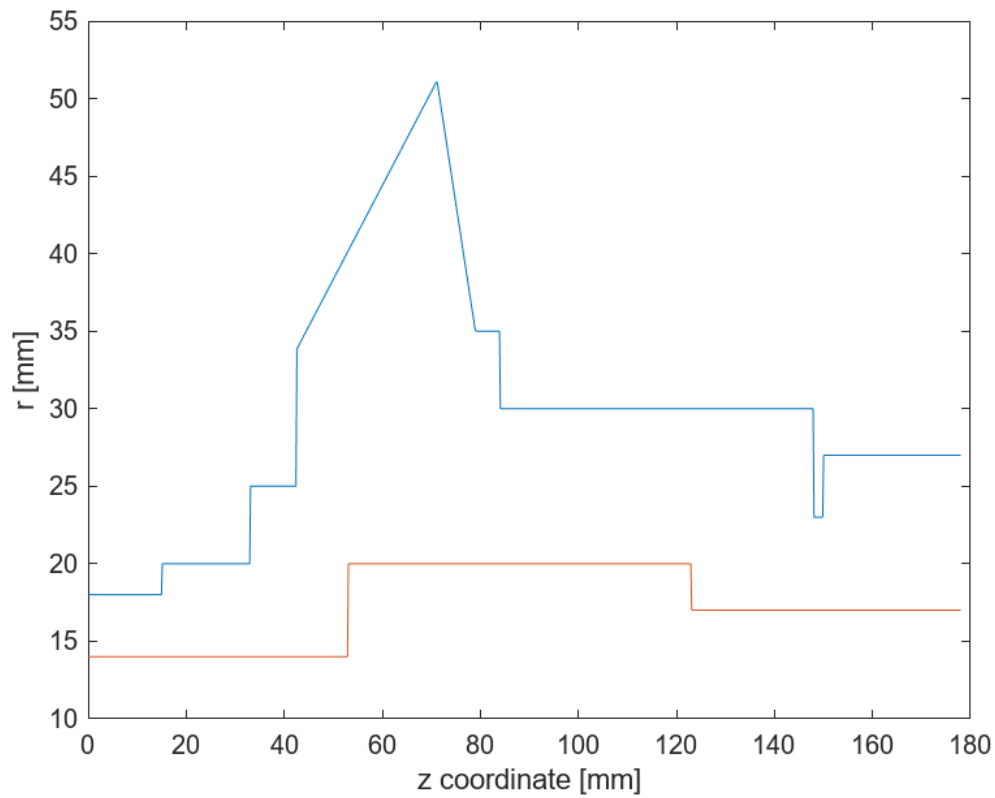


Figure 5.4 input shaft geometry

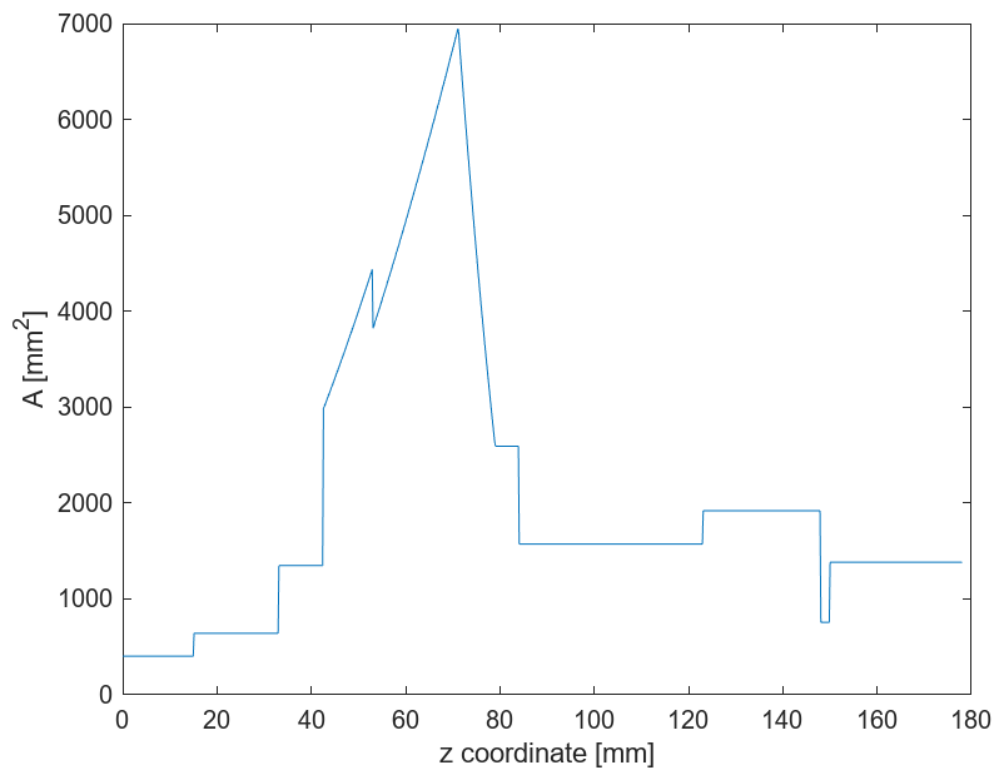


Figure 5.5 input shaft cross-sectional area values

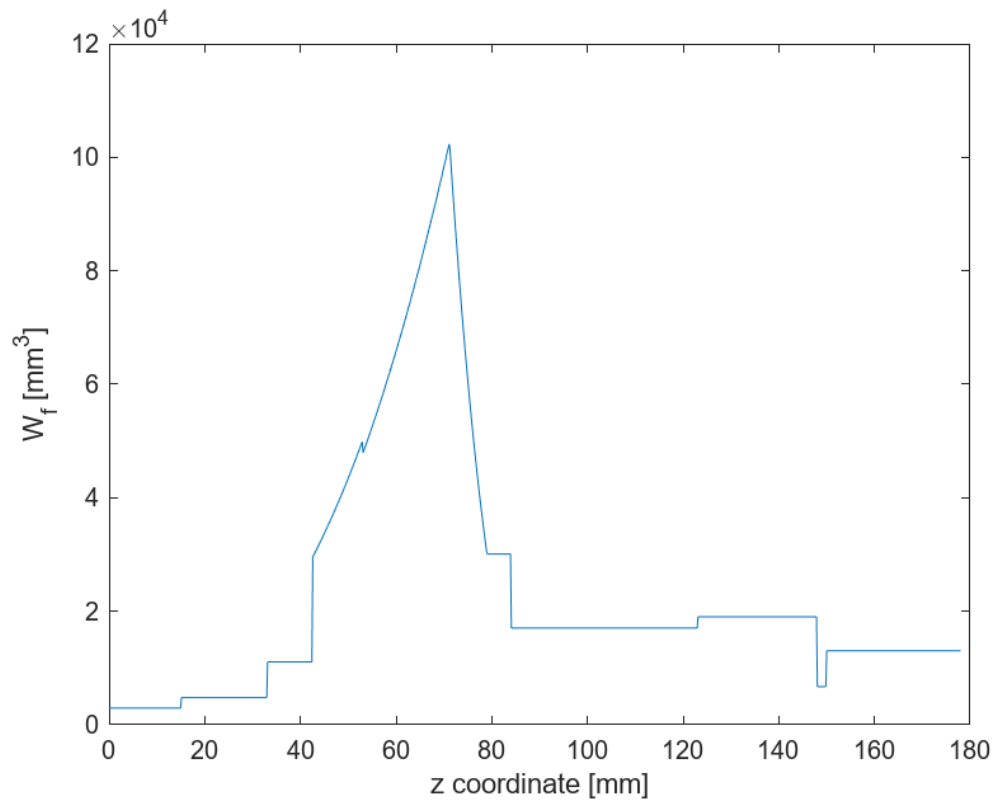


Figure 5.6 input shaft bending section modulus values

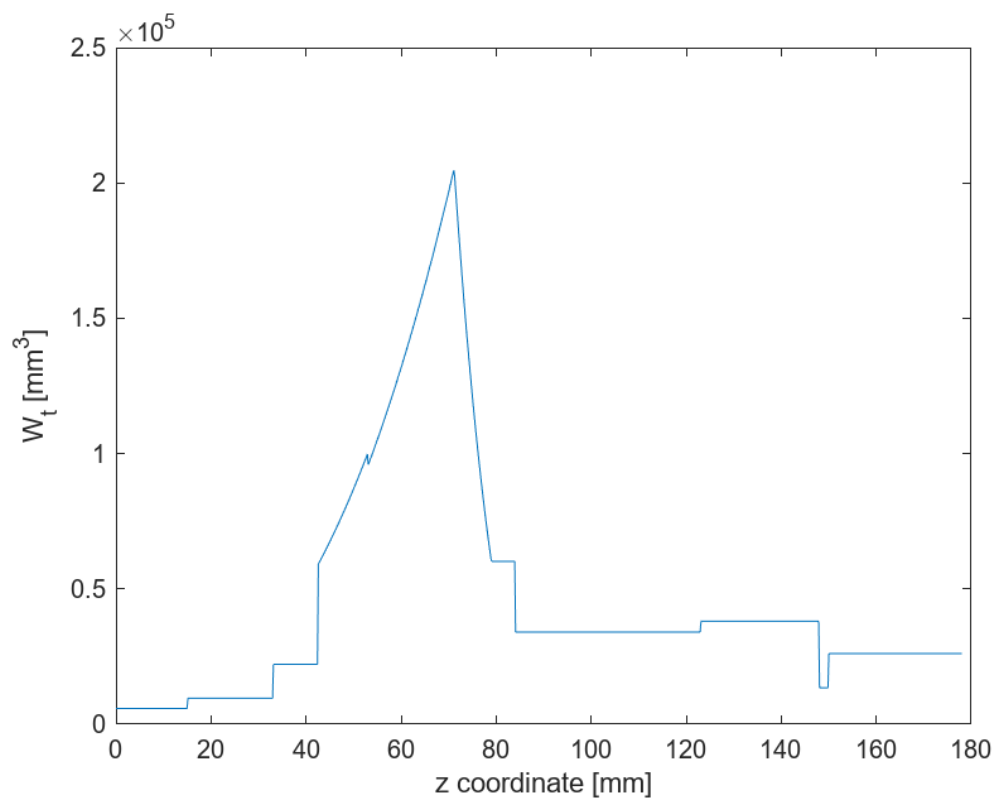
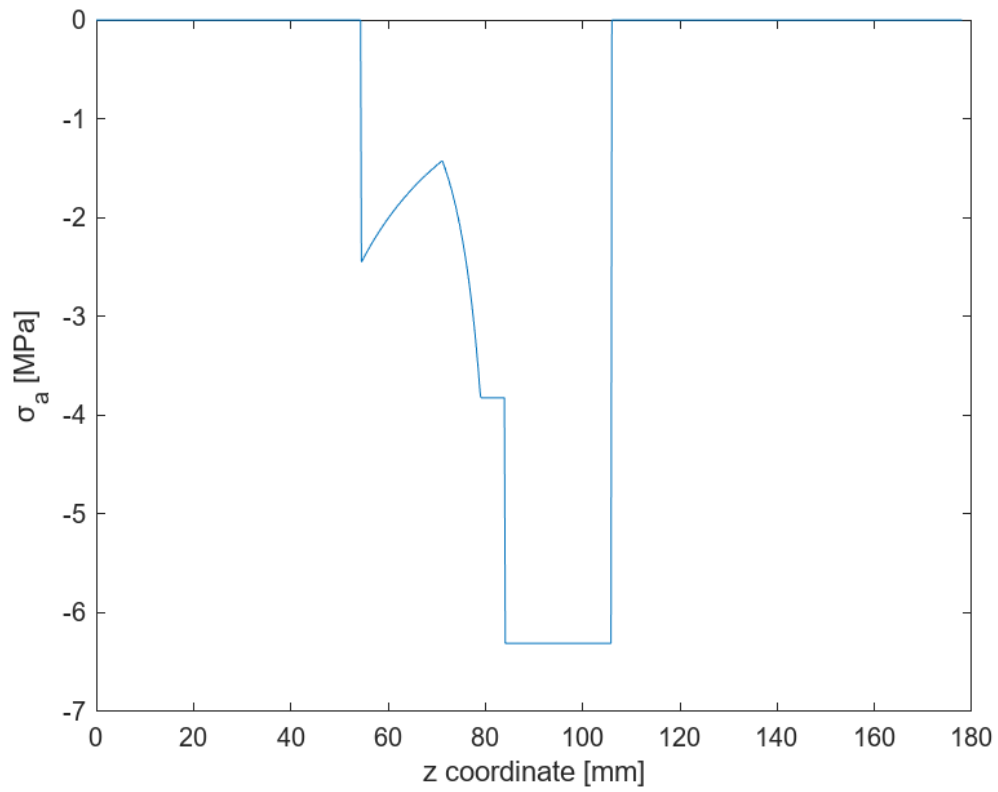
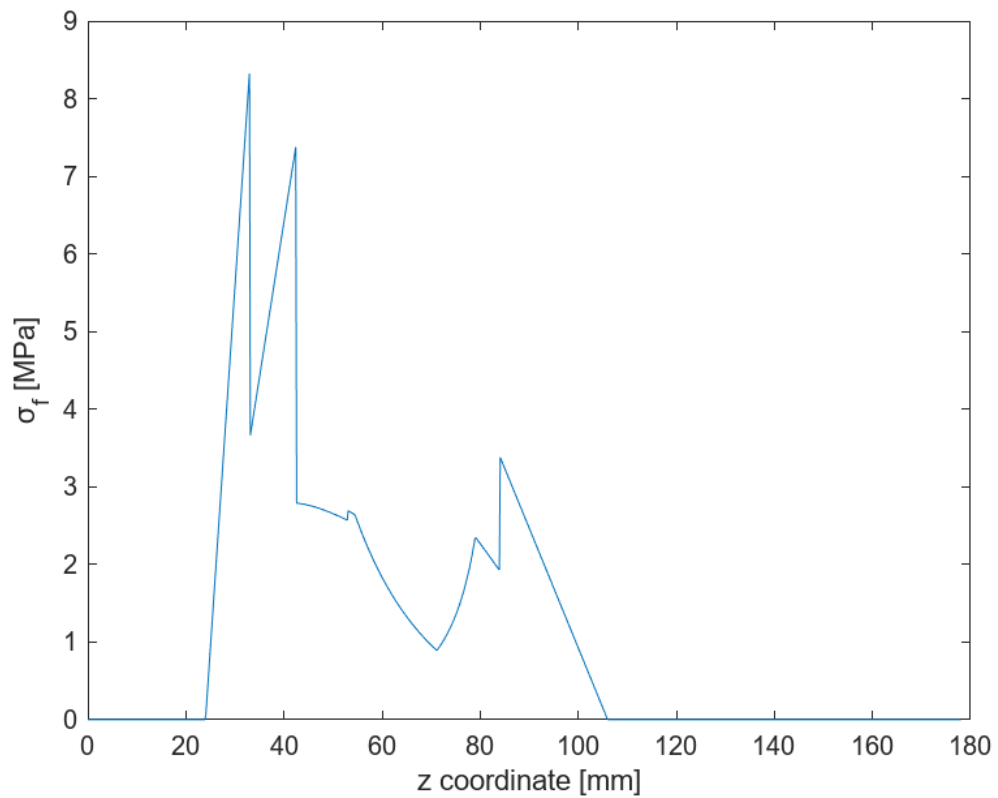
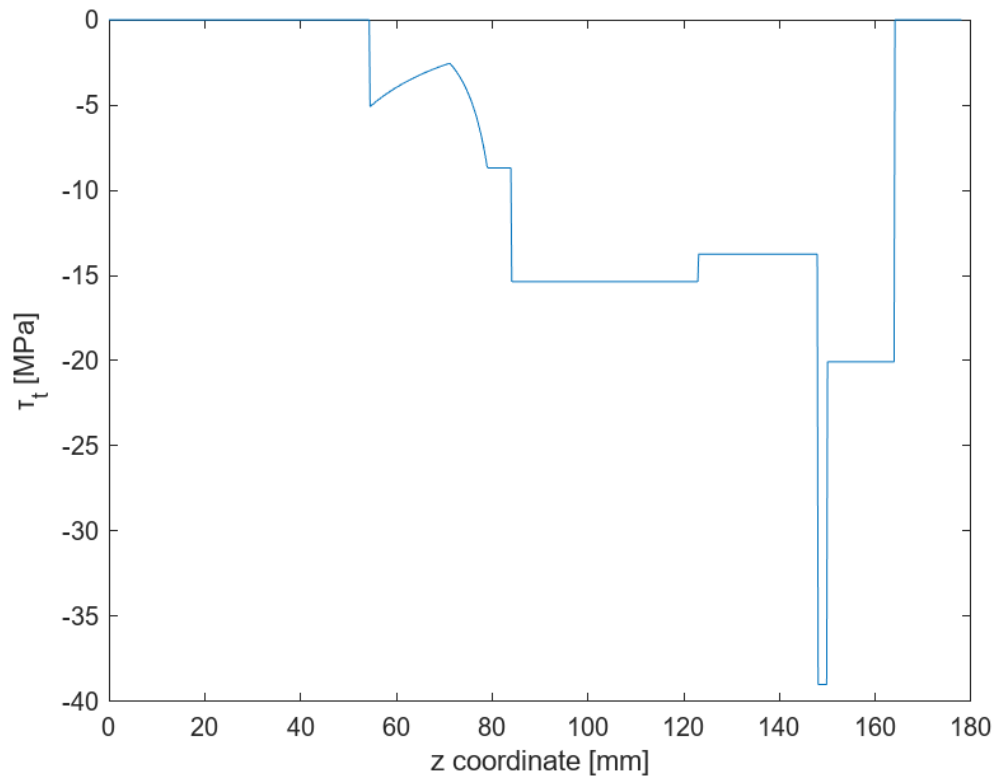


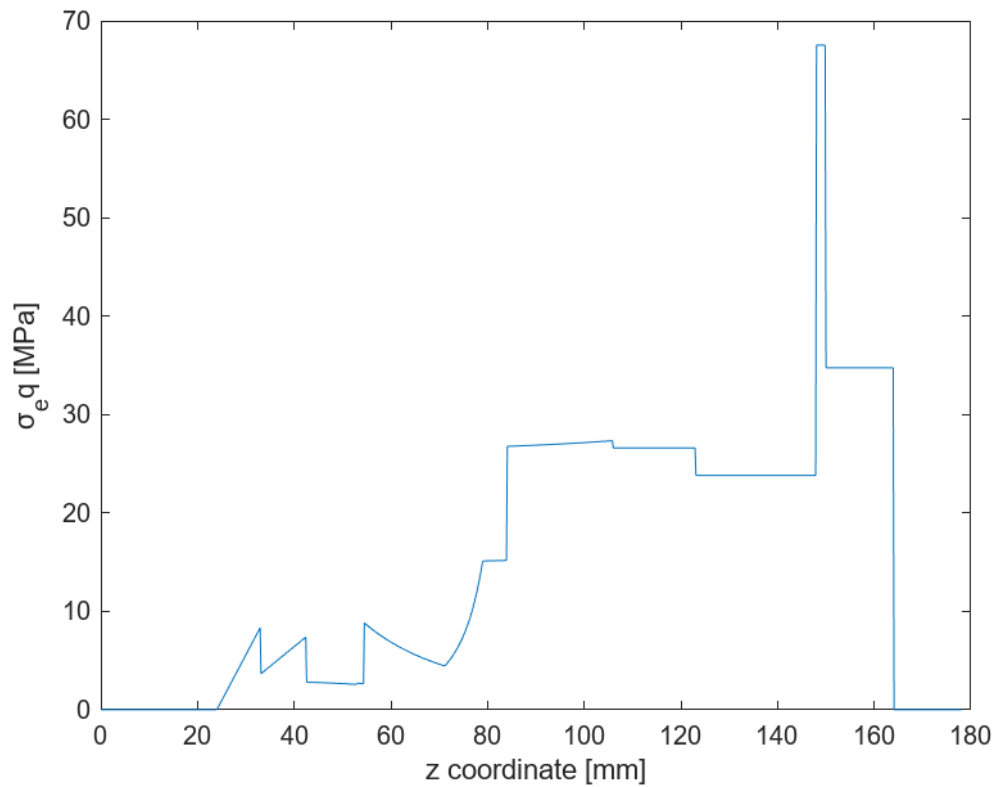
Figure 5.7 input shaft torsion section modulus values

Then the resulting stresses could be evaluated.

**Figure 5.8** axial stress**Figure 5.9** bending stress

**Figure 5.10** shear stress

Finally, the equivalent stress acting on the shaft could be computed.

**Figure 5.11** equivalent stress

From the previous figure, it is evident that the most loaded point is the point before the spline of the input coupling, where the diameter is smaller, because of the torsional stress in that part. That specific part of the shaft is not under compression or bending. Taking the stress at that point under consideration and considering the yield strength of the chosen material, the computed safety factor is equal to 18, which is much higher than the required safety factor of 3 for ductile materials such as steel. Thus, the shaft is verified for static loading.

5.2 Fatigue Verification

Following the static verification of the two shafts, the next step is to verify their operation under dynamic conditions. Since the shafts are rotating while their point of contact remains at the same place, there exists a dynamic loading condition due to the effective rotation of the bending moment, as the bending moment is not constant across the whole diameter of the shaft, unlike the normal and torsional components of the stress. Thus, the bending stress will act as an alternating stress with zero mean value, while the other two components will act as a mean stress with no alternating stress component.

The values of the stress will also be influenced by the changes in the diameter of the shaft, and the shape of the gear itself. Thus, the stress will be higher in some regions because of these inconsistencies in the shaft geometry.

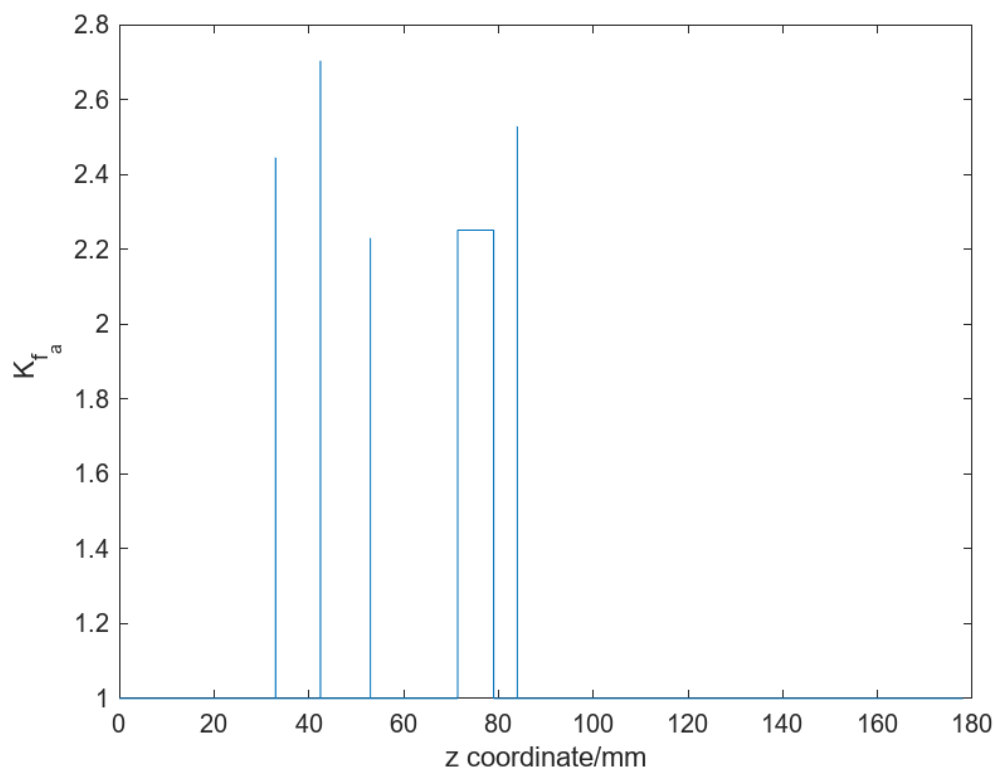


Figure 5.12 stress concentration factors for axial stress

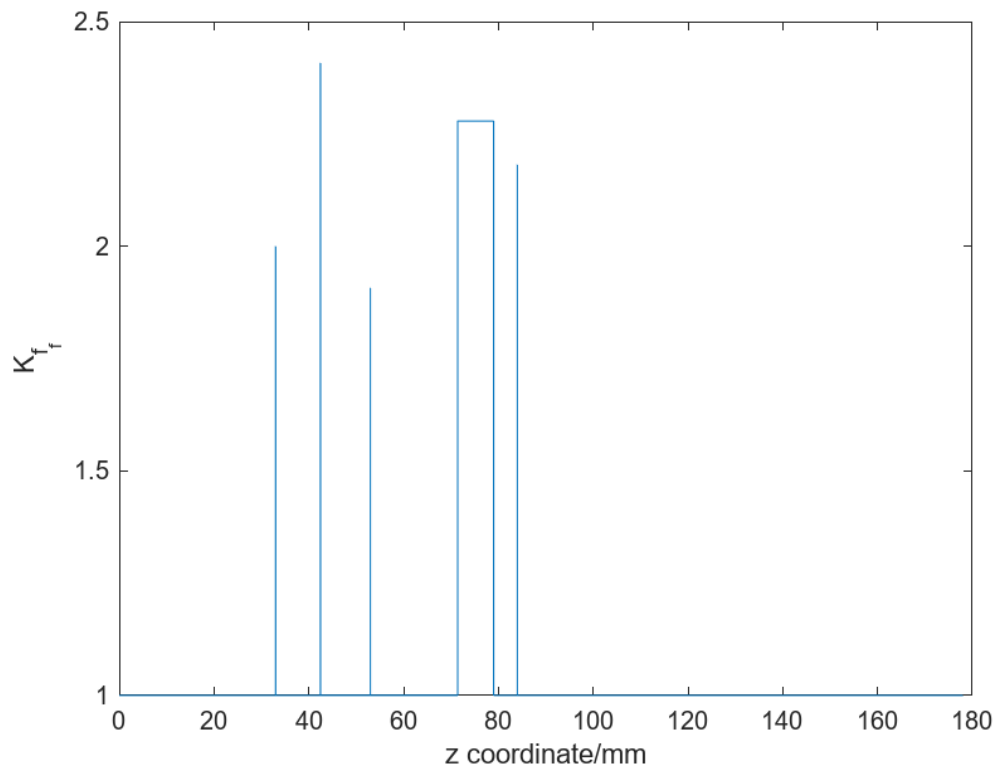


Figure 5.13 stress concentration factors for bending

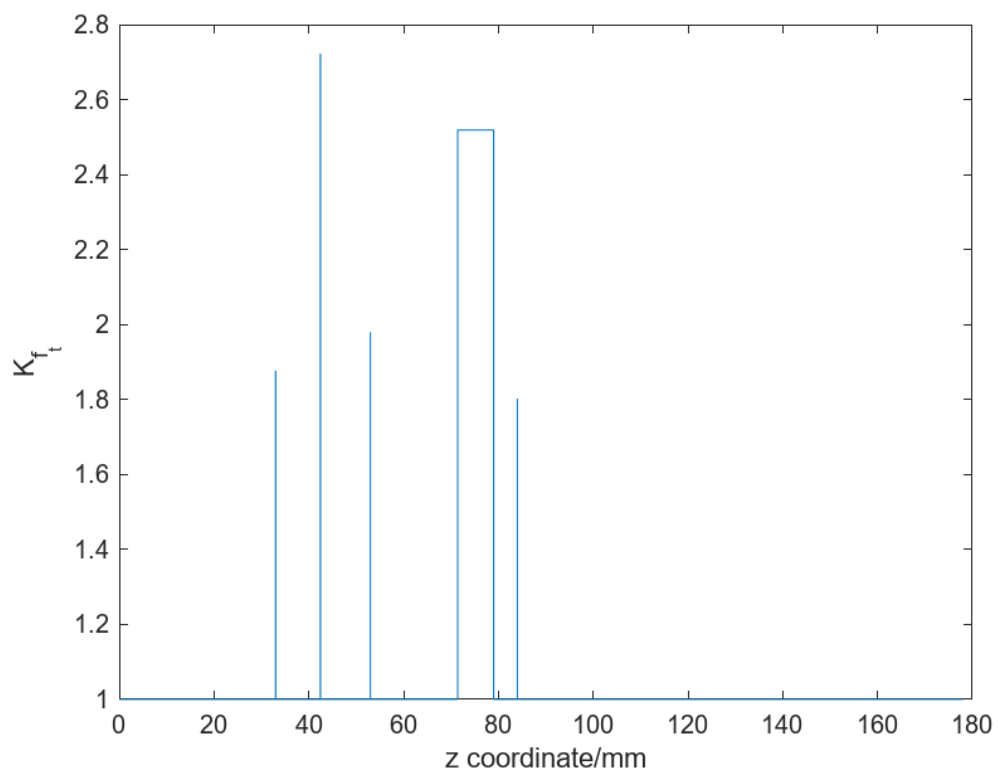


Figure 5.14 stress concentration factors for shear

The FKM standard was used to perform this part of the shaft verification. The procedure starts from nominal values of stress, from which the actual strength values are computed taking into consideration the size of the component, the anisotropy of the material, and the loading type. Using these values, the fatigue limit could also be obtained. The values of the ultimate and yield strength, and the fatigue limit are given below.

Quantity	Symbol	Value [MPa]
Ultimate strength	R_m	989
Yield strength	R_e	832
Fatigue limit of the component	$\sigma_{D-1,c}$	387

Table 5.1 Strength and fatigue limit values of the input shaft

Using these values, and applying a safety factor of 1.35, considering severe failure consequences and regular inspections, the Haigh diagram can be plotted in the next figure. As can be seen, the values of the stress are within the safety region of the diagram, even with the safety factor applied. Therefore, the shaft can be confirmed for infinite life.

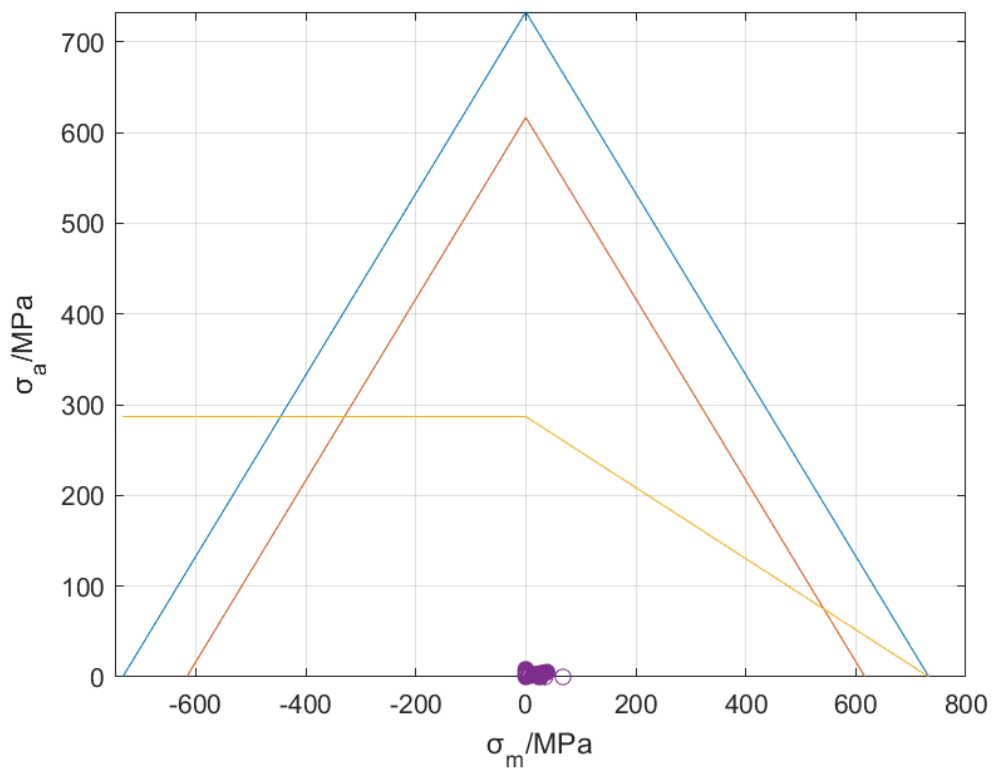


Figure 5.15 input shaft Haigh diagram

Closing Remarks

As examined in previous parts of this study, the transmission system between the main gearbox and the tail plays an important role for power transmission, speed reduction, and the regulation of the amount of antitorque produced.

The design of the system needs to consider several factors, notably, the presence of the blade pitch angle control mechanism and the required speed reduction, the connection of the shafts to the rest of the system via couplings. Consequently, the shape of the shafts is determined by the shape of the gears which are responsible for that speed reduction. Shaft geometry is also determined by the bearings required to constrain the shafts in place. Having verified the gears and the bearings for the application, the design of the shafts, the shape of the external case, the seals and the position of the threaded connections could be finalized.

When finalizing the design, several modifications were required to make the components functional from a manufacturing and maintenance point of view, for instance, the truncation of the input shaft gear in the tail rotor gearbox, to facilitate its assembly.

With the design phase concluded, static and fatigue verification procedures were performed to assess the sufficiency of the parts to handle the required loads. Throughout the verification process of the transmission system, the severity of a potential failure had to be taken into consideration. Even though this has led to conservative results, maximum operational safety has been ensured.

Annex 1

Bearing Dynamic Life Evaluation Graphs and Tables

According to ISO 281:1 2000:

$$\text{adjusted bearing life, } L_{na} = a_1 * a_{SKF} * L_{10}, \text{ where:} \quad (A1.1)$$

a_1 : reliability adjustment factor

$$a_{SKF} = a_{SKF} \left(\kappa, \eta_c \frac{P_u}{P} \right)$$

$$\text{viscosity factor, } \kappa = \frac{v}{v_1}$$

v : actual operating viscosity

v_1 : rated viscosity

η_c : contamination factor

P_u : fatigue load limit (given by bearing catalogue)

$$\text{basic bearing life, } L_{10} = \left(\frac{C}{P} \right)^p \quad (A1.2)$$

C : dynamic basic load rating (given by bearing catalogue)

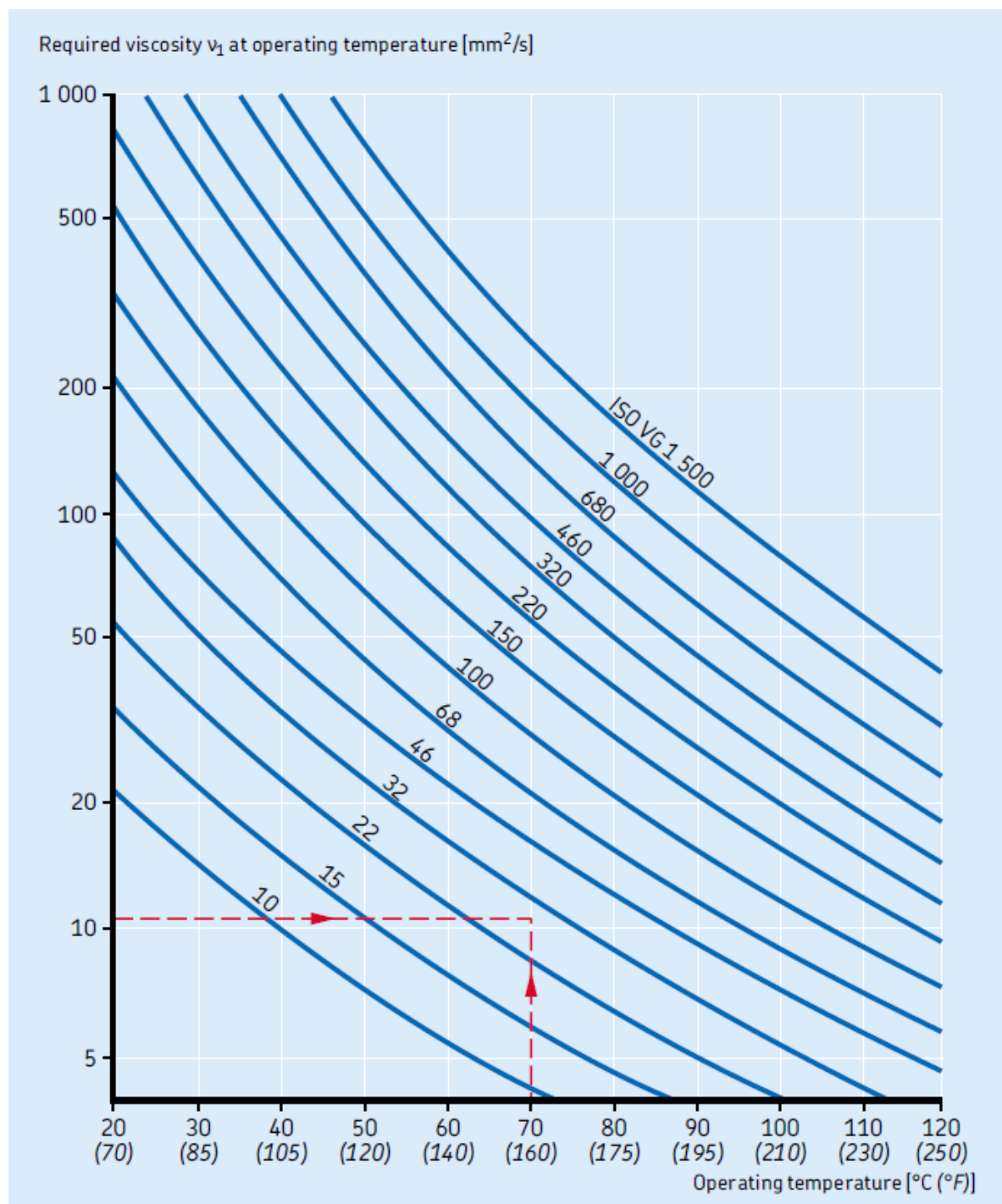
$$P = \begin{cases} XR + YA, \frac{A}{R} > e \\ R, \frac{A}{R} < e \\ A, \text{axial bearing} \end{cases} \quad (A1.3)$$

X, Y : calculation factors (given by bearing catalogue)

$$p = \begin{cases} 3, \text{ball bearing} \\ \frac{10}{3}, \text{cylindrical roller bearing} \end{cases}$$

Values for life adjustment factor a_1			
Reliability	Failure probability n	SKF rating life L_{nm}	Factor a_1
%	%	million revolutions	–
90	10	L_{10m}	1
95	5	L_{5m}	0,64
96	4	L_{4m}	0,55
97	3	L_{3m}	0,47
98	2	L_{2m}	0,37
99	1	L_{1m}	0,25

Table A1.1 a_1 values [19]

Figure A1.1 v values [19]

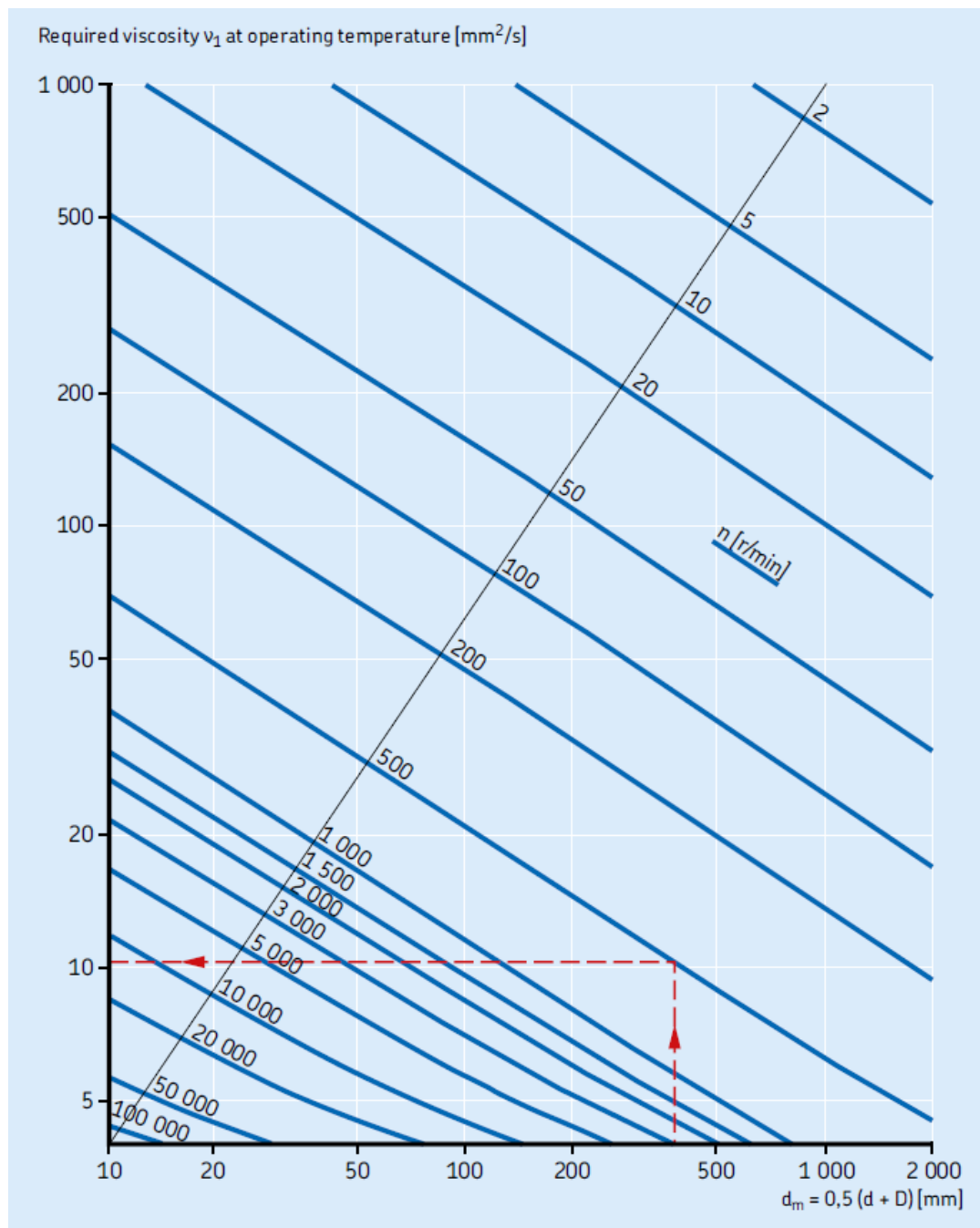


Figure A1.2 ν_1 values [19]

Guideline values for factor η_c for different levels of contamination		
Conditions	Factor $\eta_c^{(1)}$ for bearings with mean diameter	
	$d_m < 100 \text{ mm}$	$d_m \geq 100 \text{ mm}$
Extreme cleanliness <ul style="list-style-type: none"> particle size approximately the same as the lubricant film thickness laboratory conditions 	1	1
High cleanliness <ul style="list-style-type: none"> oil filtered through an extremely fine filter typical conditions: sealed bearings that are greased for life 	0,8 ... 0,6	0,9 ... 0,8
Normal cleanliness <ul style="list-style-type: none"> oil filtered through a fine filter typical conditions: shielded bearings that are greased for life 	0,6 ... 0,5	0,8 ... 0,6
Slight contamination <ul style="list-style-type: none"> typical conditions: bearings without integral seals, coarse filtering, wear particles and slight ingress of contaminants 	0,5 ... 0,3	0,6 ... 0,4
Typical contamination <ul style="list-style-type: none"> conditions typical of bearings without integral seals, coarse filtering, wear particles and ingress from surroundings 	0,3 ... 0,1	0,4 ... 0,2
Severe contamination <ul style="list-style-type: none"> typical conditions: high levels of contamination due to excessive wear and/or ineffective seals bearing arrangement with ineffective or damaged seals 	0,1 ... 0	0,1 ... 0
Very severe contamination <ul style="list-style-type: none"> typical conditions: contamination levels so severe that values of η_c are outside the scale, which significantly reduces the bearing life 	0	0

Table A1.2 η_c values [19]

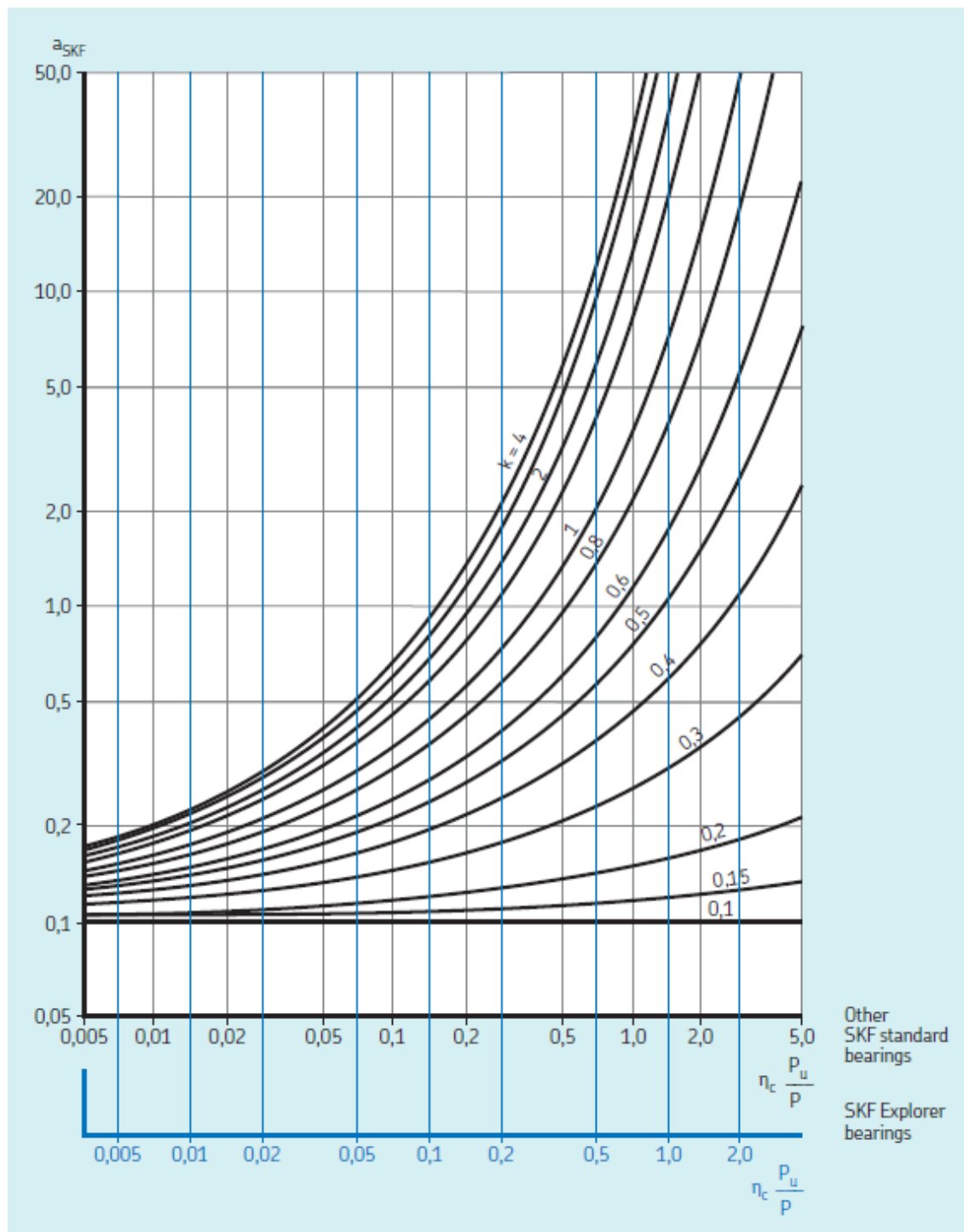


Figure A1.3 a_{SKF} values for radial roller bearings [19]

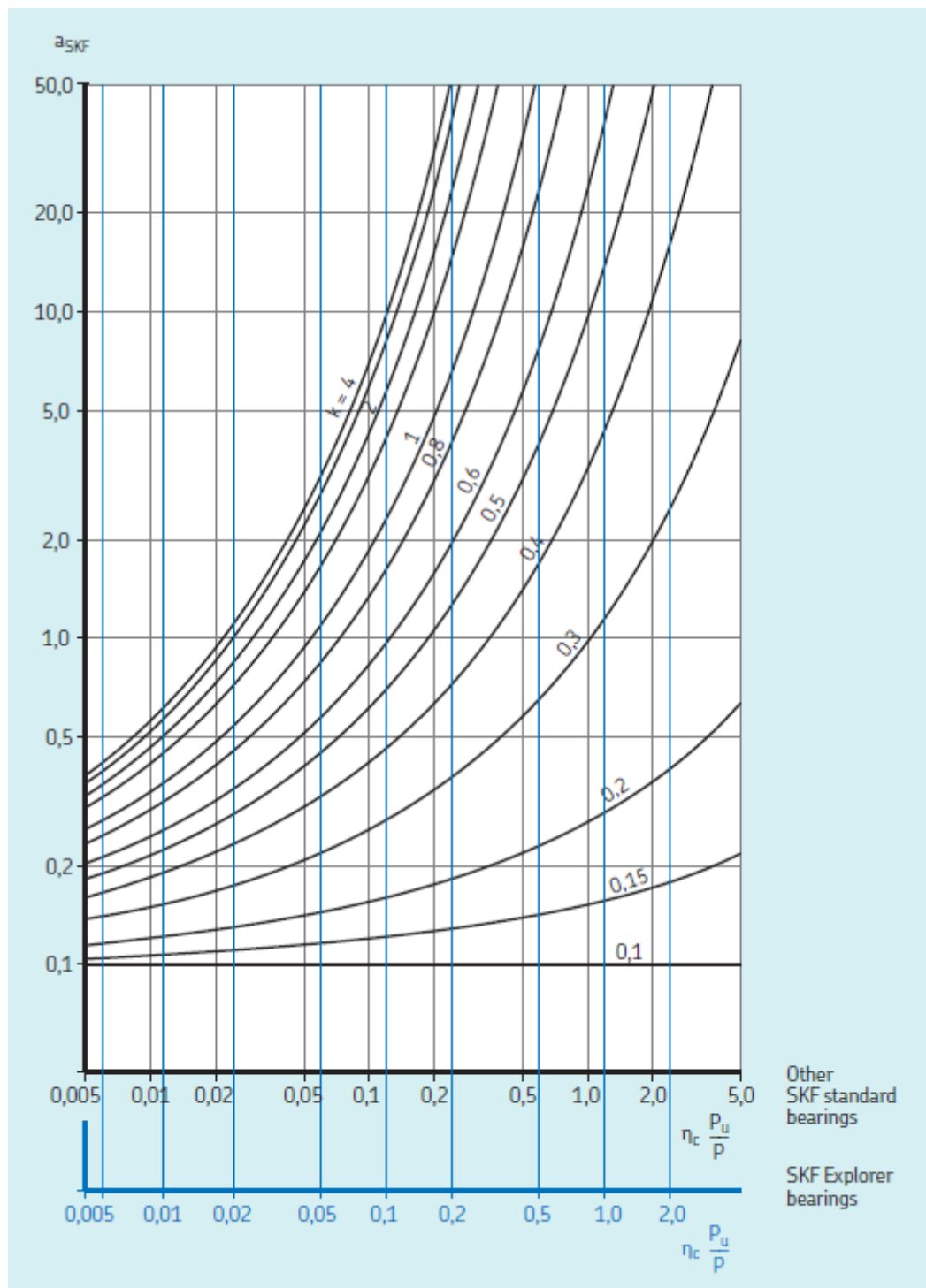


Figure A1.4 a_{SKF} values for radial ball bearings [19]

Annex 2

Graphs for Fatigue Verification

$$\sigma_{C,D-1} = b_0 * K_V * K_S * \sigma_{D-1}^{tc}, \text{ where:} \quad (\text{A2.1})$$

surface finishing coefficient, b_0 : given by FKM standard (**Fig. A2. 1**)

K_V : surface treatment coefficient

K_S : surface coating coefficient,

$$\sigma_{D-1}^{tc} = f_{w,\sigma} * R_m \text{ and } \tau_{D-1}^{tc} = f_{w,\tau} * R_m \quad (\text{A2.2})$$

$f_{w,\sigma}$: given by FKM standard (**Tab. A2. 1**)

$$R_m = K_{d,m} * K_a * R_{mN} \quad (\text{A2.3})$$

K_a : anisotropy coefficient (given by **Tab. A2. 2**)

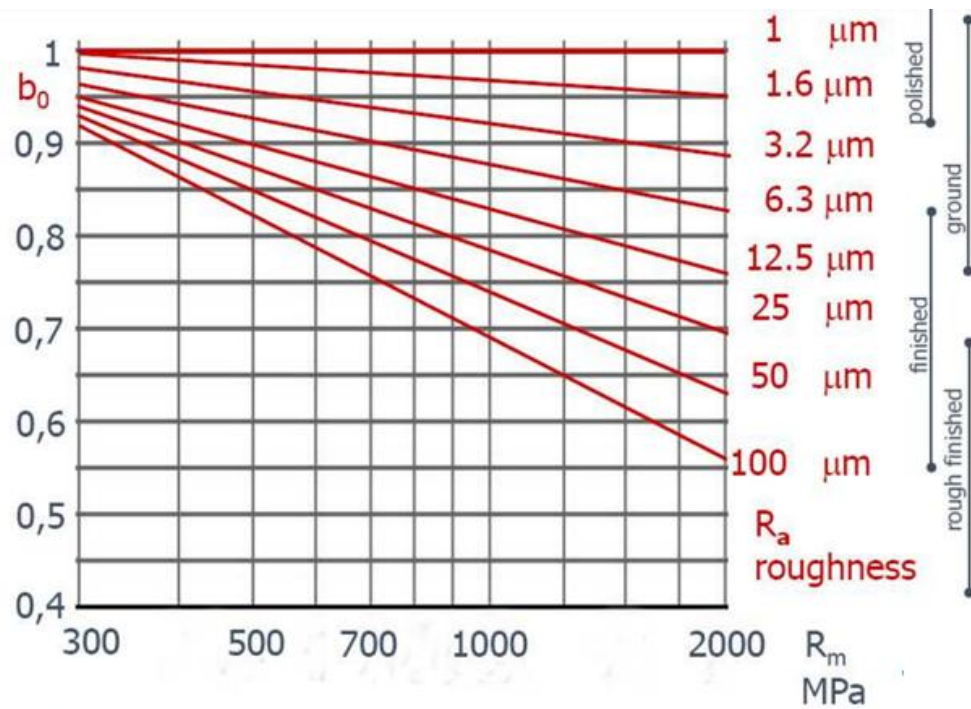
$$\text{size coefficient, } K_{d,m} = \begin{cases} 1, d_{eff} \leq d_{eff,N} \\ \frac{1 - 0.7686 * a_{d,m} * \log(d_{eff}/7.5)}{1 - 0.7686 * a_{d,m} * \log(d_{eff,N,m}/7.5)}, d_{eff,max,m} \geq d_{eff} \\ K_{d,m}(d_{eff,N,m}), d_{eff,max,m} < d_{eff} \\ > d_{eff,N,m} \end{cases} \quad (\text{A2.4})$$

$a_{d,m}$: given by FKM standard (**Tab. A2. 3**)

nominal effective diameter, $d_{eff,N,m}$: given by FKM standard (**Tab. A2. 3**)

effective diameter, d_{eff} : given by FKM standard (**Tab. A2. 4**)

maximum effective diameter, $d_{eff,max,m} = \begin{cases} 250 \text{ mm, milled steel} \\ \infty, \text{ other steels} \end{cases}$

Figure A2.1 b_0 values

Type of material	$f_{W,\sigma}^*$	$f_{W,\tau}$	Type of material	$f_{W,\sigma}$	$f_{W,\tau}$
Case hardening steel	0,40	0,577 [#]	GT- malleable cast iron	0,30	0,75
Stainless steel	0,40	0,577	GG - grey cast iron	0,30	0,85
Forging steel	0,40	0,577	Wrought alum. alloys **	0,30	0,577
Steels other than these	0,45	0,577	Cast alum. alloys **	0,30	0,577
GS – steel castings	0,34	0,577	[*] $f_{W,\sigma}$ values for $N=10^6$ cycles ^{**} does not correspond to the $N=\infty$ limit, but to $N=10^6$		
GGG – spheroidal graphite cast iron	0,34	0,65			

Table A2.1 $f_{w,\sigma}$ and $f_{w,\tau}$ for different materials

(R_m in MPa)	up to 600	from 600 to 900	from 900 to 1200	above 1200
Steel	$K_A = 0,90$	$K_A = 0,86$	$K_A = 0,83$	$K_A = 0,80$
(R_m in MPa)	up to 200	from 200 to 400	from 400 to 600	
Alum. Alloys	$K_A = 1,00$	$K_A = 0,95$	$K_A = 0,90$	

Table A2.2 K_a values

Non-alloy structural steels DIN EN 10025 (1994), grades S185, S235, S275, S355	$d_{\text{eff},N,m}=40 \text{ mm}$ $d_{\text{eff},N,p}=40 \text{ mm}$	$a_{d,m}=0,15$ $a_{d,p}=0,3$
Weldable fine grain structural steels in normalised condition DIN 17102 (1983) grades StE255 → StE500	$d_{\text{eff},N,m}=70 \text{ mm}$ $d_{\text{eff},N,p}=40 \text{ mm}$	$a_{d,m}=0,2$ $a_{d,p}=0,3$
Heat treatable steel in quenched and tempered condition DIN EN 10083-1 (1996) grades C22 → C60, 28Mn6 → 51CrV4	$d_{\text{eff},N,m}=16 \text{ mm}$ $d_{\text{eff},N,p}=16 \text{ mm}$	$a_{d,m}=0,3$ $a_{d,p}=0,4$
Case hardening steels in the blank hardened cond. DIN EN 10084 (1998) grades C10E → 14NiCrMo13-4	$d_{\text{eff},N,m}=16 \text{ mm}$ $d_{\text{eff},N,p}=16 \text{ mm}$	$a_{d,m}=0,5$ $a_{d,p}=0,5$
Spheroidal graphite cast irons DIN EN 1563 (1997) grades GJS 350-22-LT → GJS 900-2	$d_{\text{eff},N,m}=60 \text{ mm}$ $d_{\text{eff},N,p}=60 \text{ mm}$	$a_{d,m}=0,15$ $a_{d,p}=0,15$

Table A2.3 $a_{d,m}$, $d_{\text{eff},N}$ for different materials


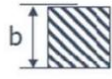



Cross section	Heat treatable steel (also forgings), case hardening steel, heat treatable cast steel, GGG, GT or GG	Non-alloyed struct. steel (also forgings), fine grained struct. steel, norm. quench. and tempered steel, Aluminium
	d	d
	b	b
	2s	s
	2s	s
	$\frac{2bs}{b+s}$	s

Table A2.4 d_{eff} for different cross-section geometries

$$\sigma_{a,eq} = \sqrt{\left(k_{f,f} * \sigma_{a,N} + \frac{k_{f,f} * \sigma_{a,f}}{0.85}\right)^2 + 3 * (k_{f,t} * \tau_a)^2} \quad (\text{A2.5})$$

$$\sigma_{m,eq} = \sqrt{(k_{f,f} * \sigma_{m,f} + k_{f,f} * \sigma_{m,f})^2 + 3 * (k_{f,t} * \tau_m)^2} \quad (\text{A2.6})$$

$$\text{notch factor for component shape, } K_f \quad (\text{A2.7})$$

$$= \begin{cases} \frac{K_t^{tc}}{n_\sigma(r)}, \text{ for tension/compression} \\ \frac{K_t^b}{n_\sigma(r) * n_\sigma(d)}, \text{ for bending} \\ \frac{K_t^t}{n_\tau(r) * n_\tau(d)}, \text{ for torsion} \end{cases}$$

K_t^{tc}, K_t^b, K_t^t : given by graphs (**Fig. A2.2**)

$n_\sigma(r), n_\sigma(d), n_\tau(r), n_\tau(d)$: given FKM standard (**Fig. A2.4**)

d : small diameter at the notch

r : notch radius

Form	$r^a)$ ± 0.1		t_1 +0.1 0	t_2 +0.05 0	f +0.2 0	g	Recommended co-relation to diameter $d_1^b)$ for workpieces	
	Series 1	Series 2					For normal duty conditions ^{c)}	With increased fatigue resistance
E		R 0.2	0.1	-	1	-	Above 1.6 to 3	-
	R 0.4		0.2	-	2	-	Above 3 to 18	-
		R 0.6	0.2	-	2	-	Above 10 to 18	-
		R 0.6	0.3	-	2.5	-	Above 18 to 80	-
	R 0.8		0.3	-	2.5	-	Above 18 to 80	-
		R 1	0.2	-	2.5	-	-	Above 18 to 50
		R 1	0.4	-	4	-	Above 80	-
	R 1.2		0.2	-	2.5	-	-	Above 18 to 50
			0.4	-	4	-	Above 80	-
	R 1.6		0.3	-	4	-	-	Above 50 to 80
	R 2.5		0.4	-	5	-	-	Above 80 to 125
	R 4		0.5	-	7	-	-	Above 125
F		R 0.2	0.1	0.1	1	(0.9)	Above 1.6 to 3	-
	R 0.4		0.2	0.1	2	(1.1)	Above 3 to 18	-
		R 0.6	0.2	0.1	2	(1.4)	Above 10 to 18	-
		R 0.6	0.3	0.2	2.5	(2.1)	Above 18 to 80	-
	R 0.8		0.3	0.2	2.5	(2.3)	Above 18 to 80	-
		R 1	0.2	0.1	2.5	(1.8)	-	Above 18 to 50
		R 1	0.4	0.3	4	(3.2)	Above 80	-
	R 1.2		0.2	0.1	2.5	(2)	-	Above 18 to 50
			0.4	0.3	4	(3.4)	Above 80	-
	R 1.6		0.3	0.2	4	(3.1)	-	Above 50 to 80
	R 2.5		0.4	0.3	5	(4.8)	-	Above 80 to 125
	R 4		0.5	0.3	7	(6.4)	-	Above 125
G	R 0.4		0.2	0.2	(0.9)	(1.1)	Above 3 to 18	-
H	R 0.8		0.3	0.05	(2.0)	(1.1)	Above 18 to 80	-
	R 1.2		0.3	0.05	(2.4)	(1.5)	-	Above 18 to 50

a) Relief grooves with radii of the series 1 are preferable.
 b) The allocation to diameter range is not applicable for short offsets and thin walled parts.
 For manufacturing reasons, it would be sensible to effect several relief grooves on a single work piece with different diameters, in the same shape and size.
 c) Type G only for work pieces with less load.

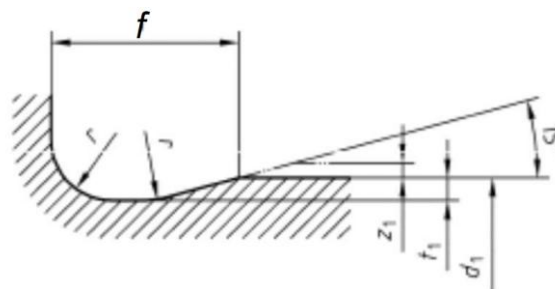


Table A2.5 relief groove dimension values

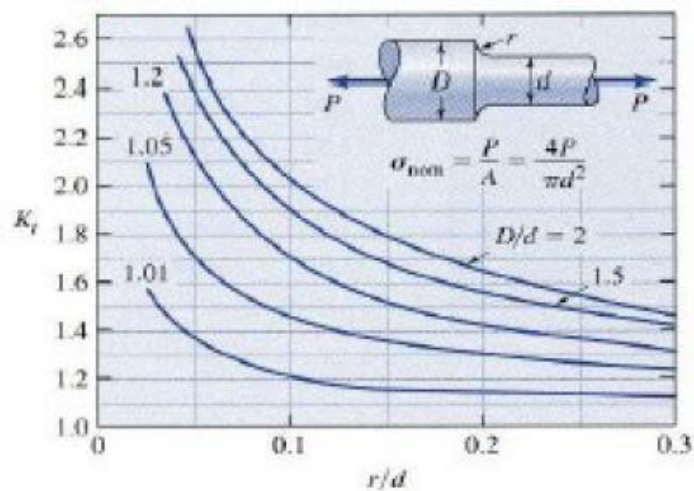
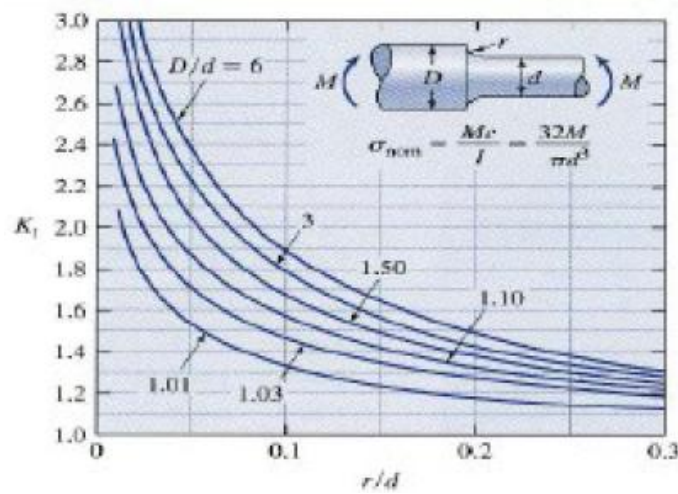
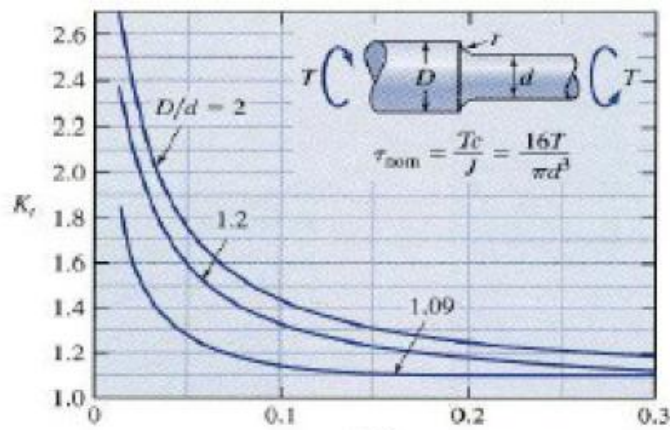
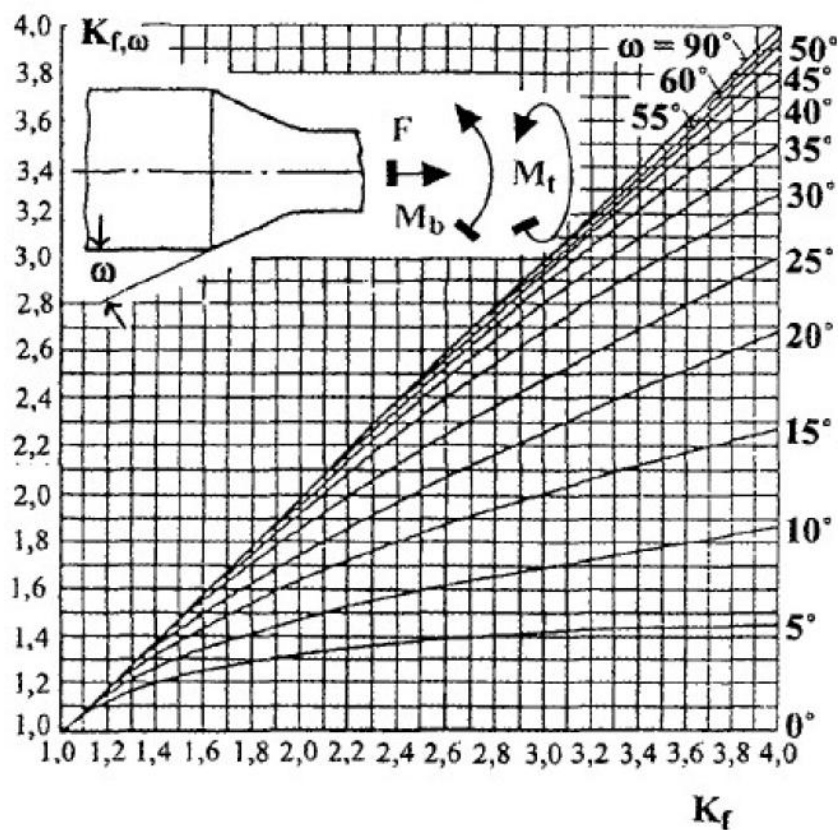
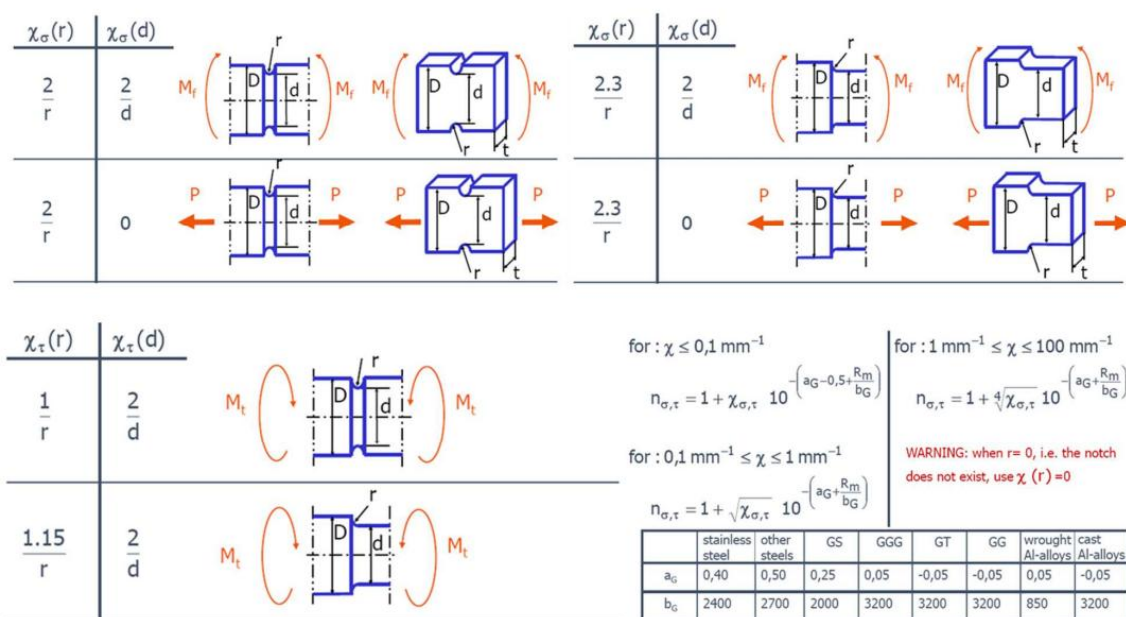


Figure A2.2 k_t values for torsion (top), bending (middle), tension/compression (bottom)

Figure A2.3 K_f value modification for conical sectionsFigure A2.4 n values for different loading conditions and component geometries

Bibliography

1. LaBerge, K.E., Ames, E.C. and Dykas, B.D., 2014. Detection of naturally occurring gear and bearing faults in a helicopter drivetrain. [online] Available at: <https://www.semanticscholar.org/paper/Detection-of-Naturally-Occurring-Gear-and-Bearing-a-LaBerge-Ames/bc256d5305d8aa4fef5307f143446955d9b00d1d>.
2. Federal Aviation Administration (FAA), 2019. *Helicopter flying handbook*. Washington, D.C.: U.S. Department of Transportation.
3. Guglieri, G., Porta, M. and Quinci, A., 2019. *Meccanica del volo dell'elicottero*. Bologna: Società Editrice Esculapio.
4. Petousis, S., 2006. *Aerospatiale SA-342L1 Gazelle*. [online] Available at: <https://www.airliners.net/photo/Cyprus-Air-Force/Aerospatiale-SA-342L1-Gazelle/1139367/L>.
5. Domke, B., 2005. *Aircraft in detail – helicopters*. [online] Available at: https://b-domke.de/aircraft_in_detail.html#Helicopters.
6. Federal Aviation Administration (FAA), 2000. *Rotorcraft flying handbook*. Washington, D.C.: U.S. Department of Transportation.
7. Huey.co.uk, n.d. *Technical manual illustrated parts assembly TO 1H-1(U)F-4*. [online] Available at: https://www.huey.co.uk/huey_servicebook.php.
8. MyMD Aero, n.d. *Helicopter spare parts*. [online] Available at: <https://www.mymd.aero/parts/541435-369d25501-9>.
9. HB Reducer, n.d. *Vent cap for gearbox*. [online] Available at: <https://hbreducer.com/vent-cap-for-gearbox/>.
10. Yin, M., Chen, X., Dai, Y., Yang, D., Xu, L. and Zhu, X., 2021. Numerical and experimental investigation of oil-guiding splash lubrication in light helicopter's reducers. *Aerospace*, 8(11), p.345. <https://doi.org/10.3390/aerospace8110345>
11. Leishman, J.G., 2006. *Principles of helicopter aerodynamics*. 2nd ed. Cambridge: Cambridge University Press.

12. Zhu, H., Chen, W., Zhu, R., Zhang, L., Fu, B. and Lu, X., 2021. Modeling and dynamic analysis of spiral bevel gear coupled system of intermediate and tail gearboxes in a helicopter. *Unpublished research paper*.
13. James, J., n.d. How Vietnam veterans are making a new home for old Huey helicopters. *HistoryNet*. [online] Available at: <https://www.historynet.com/how-vietnam-veterans-are-making-a-new-home-for-old-huey-helicopters/>.
14. Smithsonian Air and Space Museum, n.d. *Lycoming T53-L-13 LTC1K-4 turboshaft engine*. [online] Available at: https://airandspace.si.edu/collection-objects/lycoming-t53-l-13-ltc1k-4-turboshaft-engine/nasm_A19730230000.
15. Digital Combat Simulator, n.d. *UH-1H Huey Helicopter*. [online] Available at: https://www.digitalcombatsimulator.com/en/products/helicopters/huey/?PAGEN_1=3.
16. AlphaCoders, n.d. *Helicopter wallpaper*. [online] Available at: <https://wall.alphacoders.com/big.php?i=428651>.
17. NASA Airborne Science Program, n.d. *UH-1 Huey*. [online] Available at: https://airbornescience.nasa.gov/aircraft/UH-1_Huey.
18. Coe, H., 1989. Comparison of predicted and measured temperatures of UH-60A helicopter transmission. Washington, D.C.: NASA Office of Scientific and Technical Information.
19. SKF, n.d. *Rolling bearings catalogue*. [online] Available at: <https://www.skf.com/group>.
20. U.S. Army Aviation and Troop Command, 1965. *Depot maintenance work requirement for ninety-degree gearbox*. U.S. Army Publication Distribution Centers.
21. Knudsen, G.E., 1974. *R&M data analysis of the UH-1/AH-1 tail rotor system*. NTIS.
22. U.S. Army, 1998. *Aviation unit and intermediate maintenance for Army models UH60A, UH60L, and EH60A helicopters*.
23. Domke, B., n.d. *Huey helicopter images*. [online] Available at: <https://b-domke.de/AviationImages/Huey/6492.html>.
24. Challoner, N., 2019. *MD 600N photo*. [online] Flickr. Available at: <https://www.flickr.com/photos/nickchalloner/48483645906>.
25. Robinson Helicopter Company, 2016. *R44 illustrated parts catalogue*. Torrance, CA: Robinson Helicopter Company.

26. Airforce-Technology.com, 2017. *Russian Helicopters subsidiary produces first Ka-52 Alligator for 2017*. [online] Available at: <https://www.airforce-technology.com/news/newsrussian-helicopters-subsidiary-produces-first-ka-52-alligator-for-2017-5730107/?cf-view>.
27. SKF, n.d. *Tail gearbox solutions for helicopters*. [online] Available at: <https://www.skf.com/group/industries/aerospace/helicopter/transmission/tail-gearbox>.
28. SKF, n.d. *Intermediate gearbox solutions for helicopters*. [online] Available at: <https://www.skf.com/id/industries/aerospace/helicopter/transmission/intermediate-gearbox>.
29. eBay, n.d. *Bevel gearshaft image*. [online] Available at: <https://i.ebayimg.com/images/g/kkYAAOSwDC9ITxK4/s-l960.webp>.
30. GovPlanet, n.d. *Bevel Gearshaft Bell Helicopter 204-040-400-9*. [online] Available at: <https://www.govplanet.com/for-sale/Aviation-Parts-Bell-Helicopter-204-040-400-9-Bevel-Gearshaft-Unused-Nevada/2483771/NSN/3040-00-787-4269>.
31. SKF, n.d. *Main website*. [online] Available at: <https://www.skf.com/group>.
32. Han, D. and Barakos, G.N., 2017. Variable-speed tail rotors for helicopters with variable-speed main rotors. *Aeronautical Journal*, 121(1238), pp.433–448.
33. Deutsches Institut für Normung (DIN), n.d. *DIN 3990 – Calculation of load capacity of cylindrical gears*. Berlin: DIN.
34. Deutsches Institut für Normung (DIN), n.d. *DIN 3962 – Gear accuracy standards*. Berlin: DIN.
35. Federal Aviation Administration (FAA), 1998. *AC 43.13-1B – Acceptable methods, techniques, and practices – Aircraft inspection and repair*. Washington, D.C.: U.S. Department of Transportation.
36. Forschungskuratorium Maschinenbau (FKM), 2003. *Analytical strength assessment of components in mechanical engineering*. 5th ed. English version, translated by E. Haibach. Frankfurt/Main: FKM.
37. ISO (2007). *ISO 281:2007 Rolling bearings – Dynamic load ratings and rating life*. Geneva: International Organization for Standardization.